2013-01-01

A Damage-Trap Interfacial Design To Improve Impact Resistance Of Polymers

Md Shariful Islam
University of Texas at El Paso, msislam@miners.utep.edu

A DAMAGE-TRAP INTERFACIAL DESIGN TO IMPROVE IMPACT RESISTANCE OF POLYMERS

MD SHARIFUL ISLAM

Department of Mechanical Engineering

APPROVED:

Jack Chessa, Ph.D., Chair

Yirong Lin, Ph.D.

Roy Arrowood, Ph.D.

Benjamin C. Flores, Ph.D.
Dean of the Graduate School

Dedication

To my mother.

A DAMAGE-TRAP INTERFACIAL DESIGN TO IMPROVE IMPACT RESISTANCE OF POLYMERS

by

MD SHARIFUL ISLAM, B.S. ME

THESIS

Presented to the Faculty of the Graduate School of

The University of Texas at El Paso

in Partial Fulfillment

of the Requirements

for the Degree of

MASTER OF SCIENCE

Department of Mechanical Engineering

THE UNIVERSITY OF TEXAS AT EL PASO

May 2013

Acknowledgements

In the beginning I want to thank the Department of Mechanical Engineering for providing me the opportunity to pursue my masters in this university. I am grateful to the department chair Dr. Choudhuri and graduate adviser Dr. Chessa for their support at the critical moment of my research. I want to express deep gratitude to Dr. Roy Xu for his continuous support and motivation to finish my thesis. Special thanks to Dr. Lin and Dr. Arrowood for serving as my committee member. I would like to thank Dr. Roy Xu's research group for their support to complete my thesis specially Mark for helping me on my experiments, Ricardo who taught me Abaqus for simulation and Kai for his motivation. I want to thank Mr. Rashedul Hasan Sarker for his continuous support to live here in El Paso.

Last but not the least; I want to thank my parents and sisters for their continuous support and enthusiasm to complete my MS degree.

Abstract

Polymer materials such as Polycarbonate (PC), Polymethyl methacrylate (PMMA) have numerous applications in transparent armor which includes body and face shield, helmet, windows of the armored vehicle etc. The most challenging part of these applications is to ensure the safety of the people. These materials are often subjected to impact loading, so it is important to study the failure of these materials under impact loading. An experimental study has been made to investigate the impact damage in transparent layered materials. Impact experiments were carried out on various monolithic specimens and layered specimens for both two types of materials at different energy level and the damage pattern of these specimens after impact was investigated. It is found that the monolithic PMMA has greater impact resistance over layered PMMA of equal thickness at very low energy impact but at moderately high energy, the layered material has greater impact resistance. Analytical and numerical approaches were also used in this study to predict the maximum impact force and contact duration.

Table of Contents

List of Tables

List of Figures

List of Illustrations

Chapter 1: Introduction

Doctrine of fire and tactics are the driver for the development of modern armor systems. In modern battlefield there is no specific battlefront and that's why every person related to battle should use protection. Ground vehicle protection, air vehicle protection, personnel protection and protection of equipments are the common military applications for transparent armor. Riot visors which are typically made from polycarbonate are used to protect from large low-velocity projectiles which includes rocks, bottles and high velocity fragments. Windows are probably the weakest part of armored vehicles, therefore, research on high-resistance transparent armors is increasingly important for US Army and Marine [1-6], as shown in Figure 1.1. It is the focus of this thesis to study the improvement of optical plastics to impact with defect traps.

(a)

(b)

(c)

Figure 1.1: Typical Transparent Armor. (a) Face Shield and Body Shield, (b) EOD Helmet and (c) Armored Vehicle

1.1 IMPACT

When two or more bodies (at least one is moving) collides each other, then the bodies apply a very high force on each other for a very short period of time. This phenomenon is known as impact. This impact force has a greater effect on how the bodies will response rather than a comparatively lower

force applied on the body for a longer period of time. This is due primarily to the stress increases that happen when transient stress waves overlap. When the loads are slowly applied these effects are minimal.

Figure 1.2: Typical Accidents in Road.

In everyday life nothing is stationary, things are moving all the time. During moving some unexpected incident may happen such as accidents and even if it is a low velocity impact it can create internal damage that may not be visible but greatly affect the strength and performance of the material in long time.

In most of the transparent protective device such as body and face shield, helmet, armored vehicle windows are made of polymers such as polycarbonate, PMMA etc. Body and face shields are mainly used by the riot police during an unstable situation such as riot to avoid any harm from the various objects thrown to them such as a stone. Usually in these types of impact the impact velocity is small but the mass could be very high so that the overall impact energy is high.

Figure 1.3: Riot Police with Body Shield and Helmet.

1.2 CHARACTERIZATION OF IMPACT DAMAGE

Impact damage can be characterized in different ways. Based on speed, impact can characterized as low velocity impact and high velocity impact.

1.2.1 Low Velocity Impact

If the impact velocity is within 1-10 m/s then the impact is often refered low velocity impact. Richardson et al. [7] defines low velocity impact according to Sjoblom et al. and Shivakumar et al., [8, 9] where the upper limit of the velocity is up to 1 to 10 m/s. Cantwell et al.[10] also classified low velocity impact up to 10 m/s but Arbate[11] stated that if the velocity is less than 100 m/s then it can be considered as low velocity impact. It should be noted that these ranges are somewhat arbitrary. Some example of low velocity can be, walking (1m/s), running (4m/s), and speed of a car at freeway (30 m /s). Low velocity impact test can be carried out in drop weight impact machine where the striker is kept above the specimen to a certain height and then release it from there to allow it to fall freely due to gravity. The height from where the striker placed should be such that the striker gains the required

velocity just before the impact. In this case the potential energy of the striker completely converts to the kinetic energy.

The impact velocity just before the impact is given by,

$$mgh = \frac{1}{2}mv^2 \qquad (1.1)$$

$$v = \sqrt{2gh} \qquad (1.2)$$

Where, m is the mass of the striker, g is the acceleration due to gravity and h is the height of the striker from the specimen. Impacts that fall in this category have their dynamic stresses dominated by the structural deflections as shown in Figure 1,4,a and b.

1.2.2 High Velocity Impact

If the impact velocity is greater than 100 m/s then it is called high velocity impact. Some examples are speed of bullet (320 m/s), speed of rocket (3373 m/s) etc. High velocity impact test can be carried out by using gas gun or FSP (Fragment-simulating Projectile).

Based on structural response the impact can be characterized as response dominated by dilatational waves, response dominated by the contact pressure and shear waves [12]. Figure 1.4 a shows this type of response of the structure. Here mass of the striker and plate ratio plays an important role to the damage characterization.

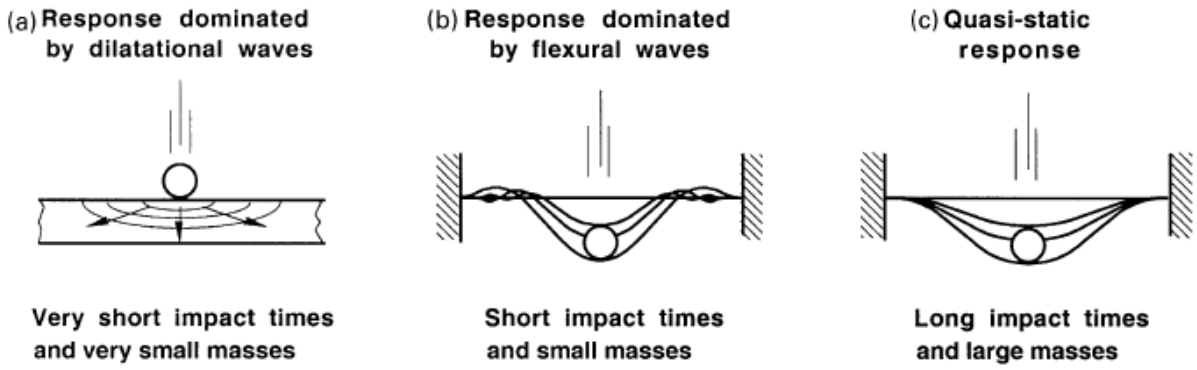

Figure 1.4: Classification of Response Types.

1.3 Preliminary Studies

More than 10 years ago, Xu and Rosakis[13] was conducting extensive impact experiments of layered materials and found some interesting results of impact resistance improvement of polymers. As shown in Figure 1.5, two layered Homalite polymers with different adhesive bonding showed very different failure patterns: dynamic cracks were trapped along the weak bonding using Loctite 5083 adhesive, which is a kind of Acetoxy silicone used mainly for potting, gasketing or sealing. Although its tensile strength and bonding strength are not high, its elongation is more than 170%.

Figure 1.6 shows a sequence of high-speed photos of the impact failure progress of the specimen with weak bond shown in Figure 1.6(b). Figure 1.6(b) reveals that the number of photo-elasticity fringes or the stress wave gradient across the weak interface (the upper horizontal line) was dramatically reduced by the thin but soft adhesive film of 20 μm in thickness. After a long time period (440 μs) of wave motion within these two layers, cracks initiated from the dark impact zone were observed near the site of impact. These crack accelerated and eventually branched as shown in Figure 1.6(c). As soon as the resulting branches approached the interface, they either arrested or turned into it producing partially interfacial debonding as shown in Figure 1.6(e). The exact reasons of the inability of these cracks to penetrate the weak bonding are complex. However, the pivotal role of the weak interface in triggering this behavior is clearly evident. This may provide a useful design methodology to prevent the spread of impact damage resulting from low speed projectiles. Figure 1.6(f) is a YouTube video based on high-speed photos obtained from one impact experiment. If we keep the same loading and material conditions except the location of the weak bonding as shown in Figure 1.7(a), dynamic cracks were still trapped by this weak interface, very similar to Figure 1.5(b). If we increased the impact speed from 20m/s to 46m/s, dynamic cracks still cannot penetrate the weak interface as seen in Figure 1.7(b). These promising results are very helpful to design new layered transparent armors with high-impact resistance using an efficient way, i.e., implanting special adhesive layers inside the polymer systems. However, fundamental failure mechanics issues of the crack trapping are not clear so far. For example, which parameter plays the major rule for crack arrest—the density, the low bonding strength, the high failure elongation of the 5083 adhesive, or the stress wave mismatch of the adhesive with the bulk polymers, or the dynamic stress intensity reduction when the dynamic crack approaches the weak bond? Obviously,

any answer will lead to better material designs. Here, we do not design materials or use this 5083 adhesive for armor systems.

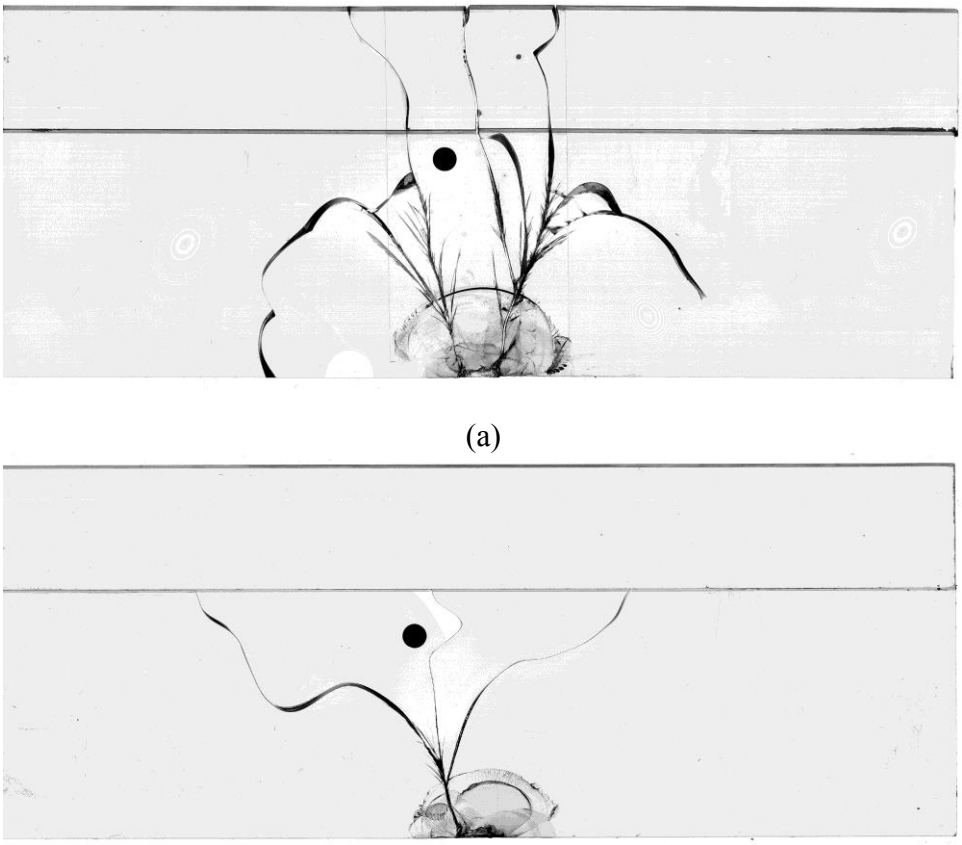

(a)

(b)

Figure 1.5: Post-mortem failure patterns of two identical brittle polymer specimens (Homalite) with different interfacial bond strengths subjected to the same impact speed of V=20 m/s. (a) 384 intermediate strength bonding (b) with 5083 weak bonding [13]

1.2 Research Objectives

1) Conducting systematic impact experiments on layered transparent polymers with new interface design, support and loading conditions to seek the high impact resistance.
2) Simulating the impact experiments to discover some key material or mechanics parameters in governing crack arrests for future armor designs.

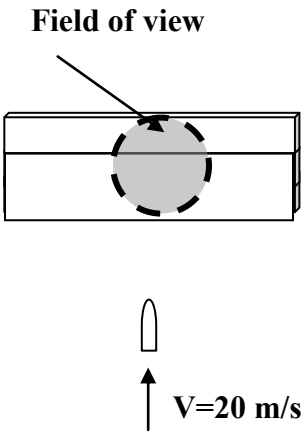

(a)

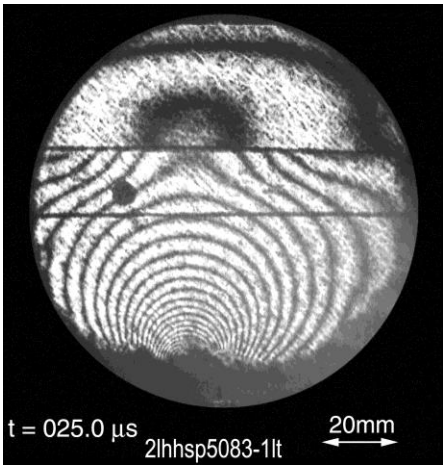

(b)

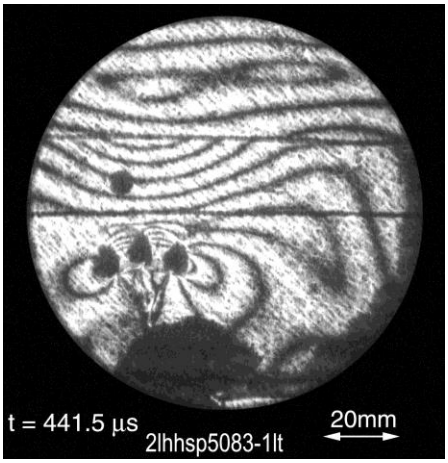

(c)

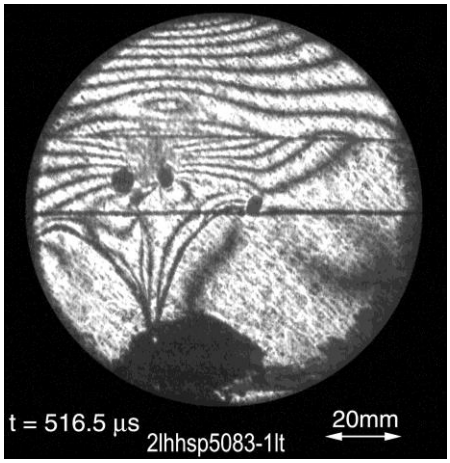

(d)

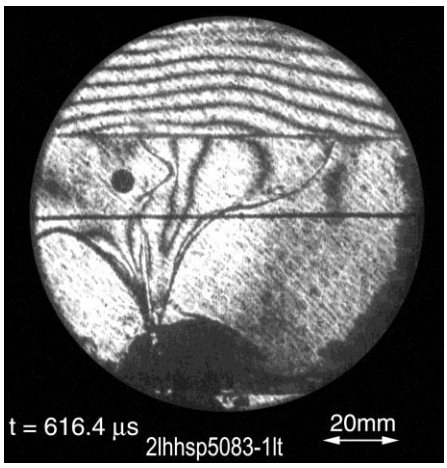

(e)

A YouTube video based on high-speed photography--------click this link

http://www.youtube.com/watch?v=5EDG2VZXaQ8&feature=plcp

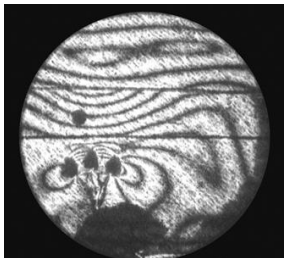

(f)

Figure 1.6: Crack propagation and arrest at a two-layer brittle polymer specimen with 5083 bonding. The central black line is the camera reference line. The upper horizontal line is the weak interface [13]

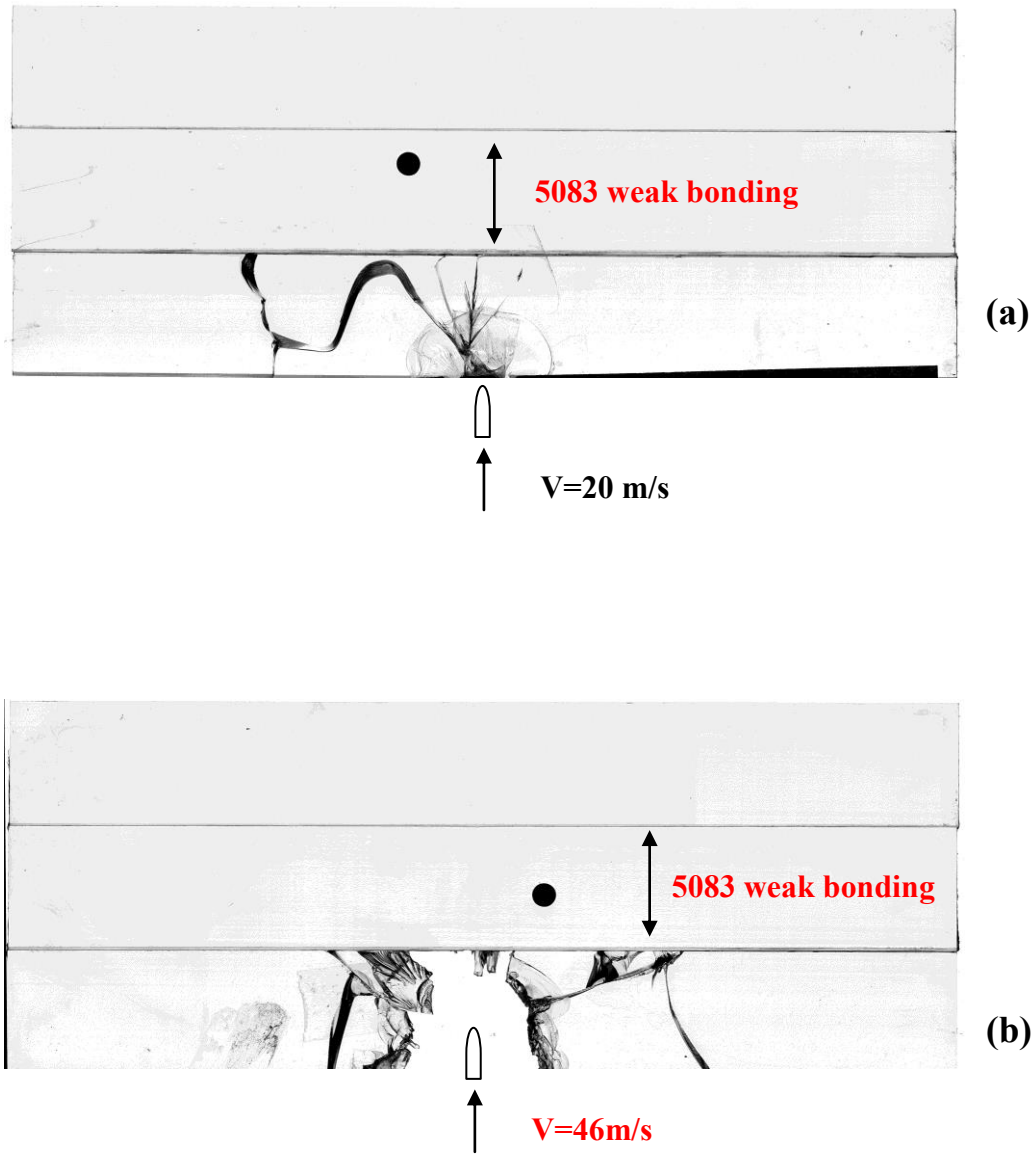

Figure 1.7: Effect of the impact speed on the failure patterns of two same three-layer polymer specimens featuring weak but ductile adhesives. Impact damage still arrested at the bonding.

Chapter 2: Experimental Program

2.1 Materials and Specimens preparation

Polycarbonate and Polymethyl methacrylate (PMMA) was selected as material for our experiments. These materials along with Polyurethane used in numerous applications in Army such as, Face shield and body shield, EOD Helmet, Army ground vehicles etc [5, 6, 14, 15]. Table 2.1 shows the typical properties of these materials. These material properties were taken from [14, 16].In this research we focused our attention to the dynamic failure of layered material under impact loading. To bond the different layers of these materials we have used Loctite 5083 adhesive. Typical properties of Loctite 5083 are given in table 2.2. Loctite 5083 provides a weak bonding between the surfaces, it is also considered as a ductile adhesive since its elongation at failure (as measured by the manufacturer) in cured bulk form is 170% or two orders of magnitude higher than the rest of the adhesives. The final adhesive thickness is about 0.55± 0.05 mm.

Table 2.1: Typical Properties of Polycarbonate and PMMA [14, 16]

Property	Polycarbonate	PMMA
Density (kg/m3)	1200	1190
Elastic Modulus (GPa)	2.38	3.79
Poisson's Ratio	0.37	0.37
Tensile Strength (MPa)	62	79
Shear Strength (MPa)	41	40
Shear Modulus (MPa)	1000	1151
Compressive Strength (MPa)	83	124
Compressive Modulus (MPa)	1660	3030
Flexural Strength (MPa)	104	104
Flexural Modulus (MPa)	2586	3280

Two different types of specimen used in experiments. Figure 2.1 shows the illustration of these two types of specimens. In type A, two layers of equal thickness PMMA used and in type B, two layers of unequal thickness (2 times than other) used. For all specimens, the length and width are equal and it is 127 mm, the only difference in these specimens is their thickness.

Table 2.2: Typical Properties of Loctite-5083 Adhesive

Property	Loctite-5083
Elongation (%)	170
Tensile Strength (MPa)	3.1
Tear Strength (N/mm)	9.4

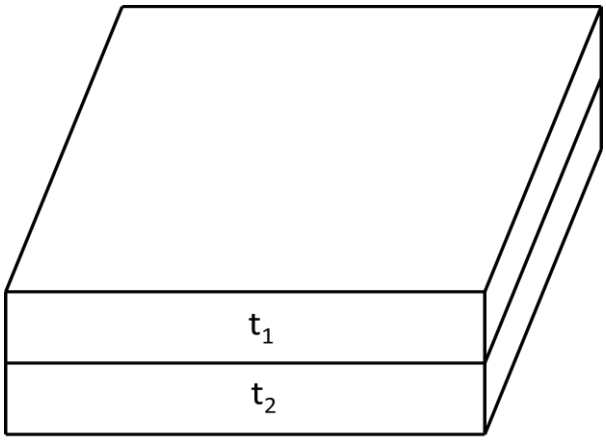

(a)

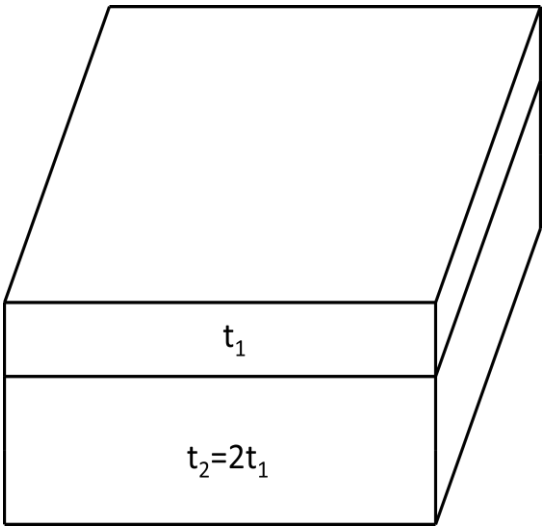

(b)

Figure 2.1: Model Specimen Geometries, (a) two layers with equal thickness (type-A) and (b) two layers with $t_2=2t_1$ (type-B).

Figure 2.2 shows the actual bonded specimens. During bonding special care have been taken to avoid any air bubbles in the interface, because if there are any bubbles inside the interface then it can work as a micro-crack which might initiate the damage and also bubbles would degrade transparency. After bonding, the specimens have cured with a UV light (intensity 225 mW/cm2 and wavelength 365nm) as recommended by the manufacturer. After UV curing the specimen was then left for 7 days in normal atmospheric condition for further curing.

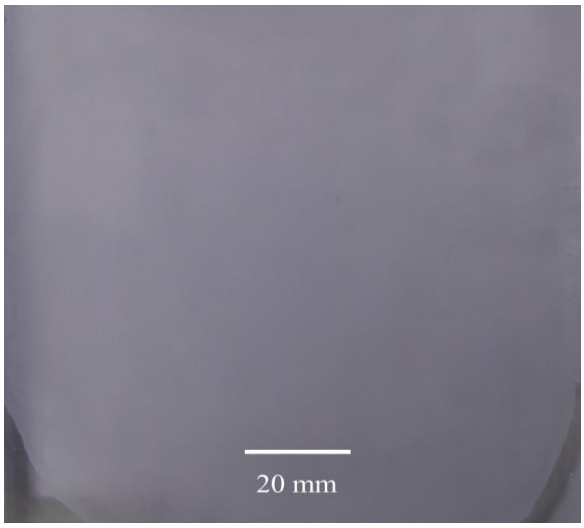

(a)

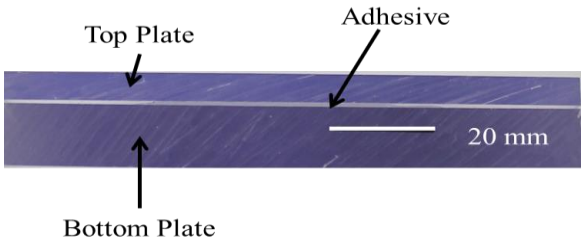

(b)

Figure 2.2: Bonded Specimen (a) Top View and (b) Side View.

2.2 IMPACT TEST PROCEDURE

Impact tests were carried out in a drop weight impact machine. Figure 2.3 shows the schematic diagram of a drop weight impact machine. Figure 2.4 shows the test section of the impact machine. The specimen kept in a fixture which was attached over a fixed stand. The figure also shows the clamping

device used to clamp the specimen over the fixture. This clamp applies a pressure of about 0.5 MPa to the top surface of the specimen to hold it tightly over the fixture. All the tests were carried out with a steel striker of mass 3.105 kg. The machine automatically adjusts the initial height of the striker for different energy level. At first the impact test were carried out at different energy level on a single PC or PMMA plate to find the critical impact energy in which energy the crack initiates. Then the impact tests were carried out on the bonded specimen at the same impact energy.

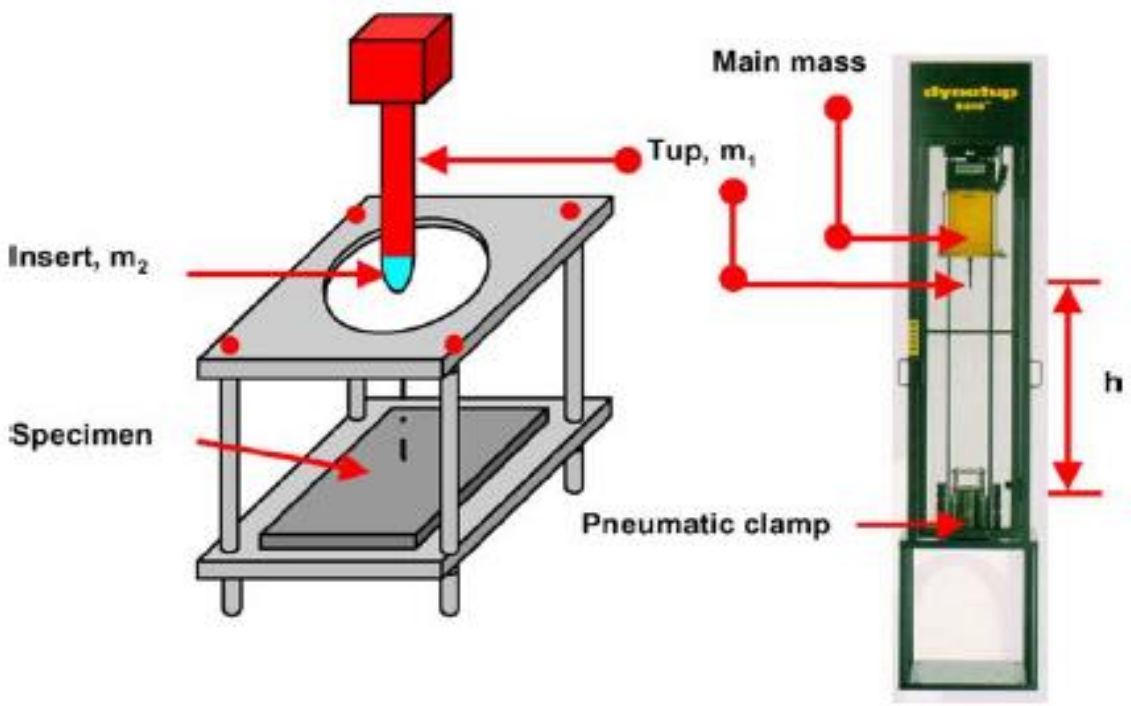

Figure 2.3: Schematic Diagram of an Impact Machine.

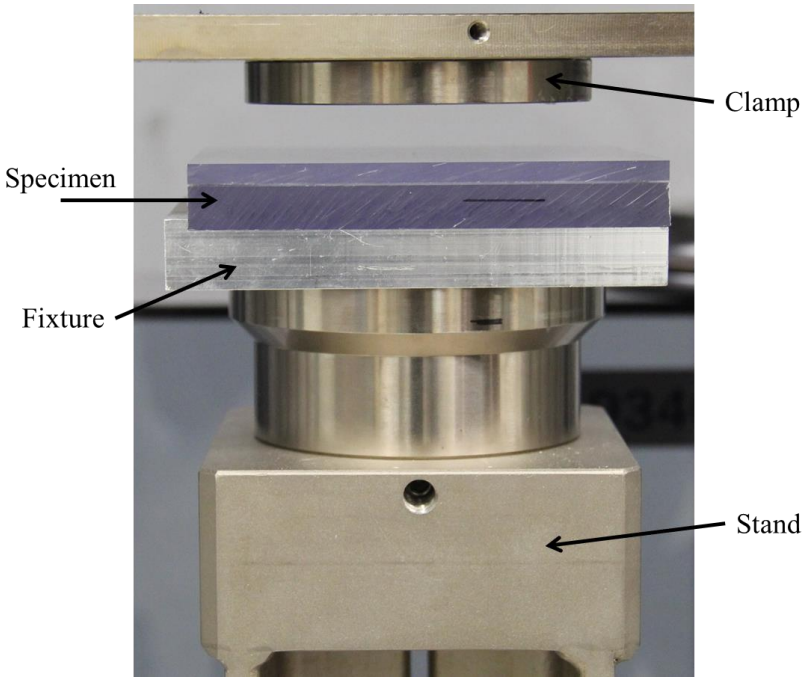

Figure 2.4: Test Section of Impact Machine.

Chapter 3: Modeling and Simulation

3.1 THEORETICAL MODEL

3.1.1 Indentation mechanics for both static and dynamic indentation processes

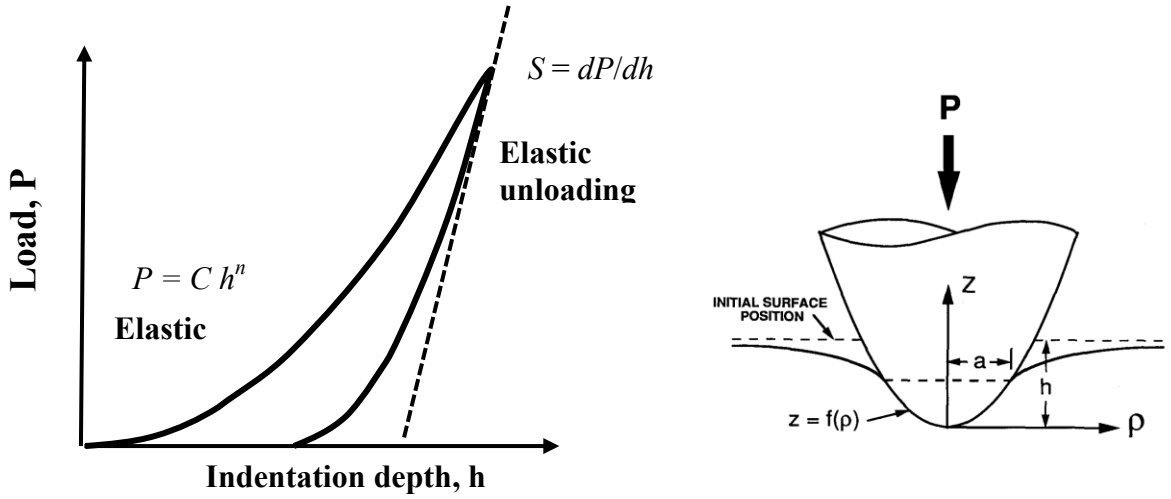

Figure 3.1: A typical load-displacement curve for an indentation process.

As shown in Figure 3.1, the indentation load P of a spherical indenter is a function of the indention depth h and the indenter radius R based on Hertz's contact law[17, 18]:

$$P = \frac{4}{3}\sqrt{R}\,E_r\,h^{\frac{3}{2}} = C_{ID}\,h^{\frac{3}{2}} \tag{3.1}$$

Where C_{ID} is the contact stiffness for a nano-indentation process; and the reduced modulus E_r is determined by the Young's modulus E and the Poisson's ratio v for the isotropic and homogenous target materials, as in

$$\frac{1}{E_r} = \frac{1-\nu_i^2}{E_i} + \frac{1-\nu^2}{E} \tag{3.2}$$

Where the subscript i refers to the indenter.

3.1.2 Dynamic indentation and impact processes

During a dynamic indentation process (cf. Figure 3.2), the total force acting on the indenter is the indentation force from the target only. Thus, we have

$$\sum F = P = ma \quad \Rightarrow \quad m\ddot{h} + Ch^{3/2} = 0. \quad (3.3)$$

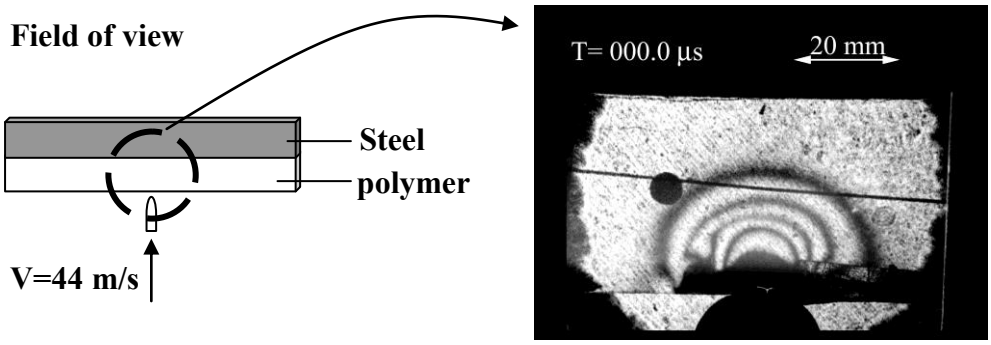

Figure 3.2: A dynamic indentation process of a steel projectile on a layered material. Impact damage initiated from the polymer layer based on high-speed photography

The maximum impact force is achieved at the zero speed of the indenter (projectile), and is simply determined using the impact energy (W) of the indenter/projectile, and the contact stiffness between the indenter and the target (C_{IP}), as in [18]

$$P_{\max} = C_{IP} h^{3/2} = 1.14\sqrt[5]{E^3 C_{IP}^2}\,. \quad (3.4)$$

The contact stiffness of impact has the same form with the nano-indentation case; and based on Hertz's contact law with different length-scales (with indenter radius being R_{IP}), we have [18]

$$C_{IP} = \frac{4}{3}\sqrt{R_{IP}}\, E_r^{IP}. \quad (3.5)$$

3.1.3 A novel approach: Use length-scale relationship of indentations to estimate the maximum force

Based on the relationships provided above, the contact stiffness of impact (C_{IP}) can be obtained from the nano-indentation test for the same target material system (i.e., C_{ID}) based on a scaled relation,

$$C_{IP} = C_{ID}\sqrt{R_{IP}/R_{ID}}\left(E_r^{IP}/E_r^{ID}\right). \qquad (3.6)$$

For composites, steel projectile impact, and a diamond nano-indenter, we have $E_r^{IP}/E_r^{ID} \approx 0.9$. Given the above observation (i.e., Eq. 3.6), we propose to construct an efficient procedure that circumvents impact testing with which damage initiation and maximum damage can be easily determined.

It is important to note that the strain rate effect is not an issue in our experimental studies. For some—although not all—materials, the strength or fracture toughness will indeed generally increase with the increase of the applied strain rate. However, based on extensive experimental results, the strain rate is well known to have the least effect on stiffness, as described in Eq. (3.6).

3.1.4 Energy Balance Model

A very useful approach to study impact dynamics is to consider the balance of energy of the system. The deformation of the structure is resulted from the kinetic energy of the projectile [18]. The kinetic energy of the projectile is used to deform the structure and thus the maximum deformation of the structure occurs when the kinetic energy of the projectile becomes zero. The deformation of the structure may include bending, shear deformation and if the deformation is large then it may include membrane stiffening effect. If the impact energy is such that it creates very small amount of damage to the structure then the energy required to create damage can be neglected. So the energy balance equation can be written as[18]

$$\frac{1}{2}MV^2 = E_b + E_s + E_m + E_c \qquad (3.7)$$

Where E_b, E_s and E_m refer to the energy used in bending, shear and membrane deformations respectively. E_c is the energy stored in the contact region during indentation.

The Hertz contact law can be expressed [18]

$$P_{max} = C_{IP}h^{3/2}$$

If the impact structure is thick and deformation of the structure is negligible, then it can be considered that all the kinetic energy is used to indent the structure.

From which the maximum contact force becomes [18],

$$P_{max} = 1.14(E^3 C_{IP}^2)^{0.2} \qquad (3.8)$$

Where, E is the kinetic energy of the projectile.

And the contact duration is given by [18],

$$T_C = 3.529(E^2 V^{-5} C_{IP}^{-2})^{0.2} \qquad (3.9)$$

3.2 NUMERICAL SIMULATION

A dynamic explicit finite element simulation was carried out in available commercial software Abaqus 6.11 to help in the understanding of the basic mechanics of the problem. The model is discussed in the following section.

3.2.1 Modeling of Target Plate

The problem can be treated as a 3 dimensional axisymmetric problem where the stress varies along the radial direction from the center. The target plate was a 3D deformable object (PC or PMMA) with a material property as mentioned in table 2.1. C3D8R elements were used to mesh the PC or PMMA plate which is 3D 8 node element with reduced integration and hourglass control. Figure 3.1 shows the top view of the mesh on PC or PMMA plate. A very fine mesh were used in the center (at the impact area) to capture various parameters accurately and gradually decreased resolution of mesh were used outside of the impacted area. Figure 3.2 shows the enlarged view of Figure 3.1.Figure 3.3 shows the mesh from side view.

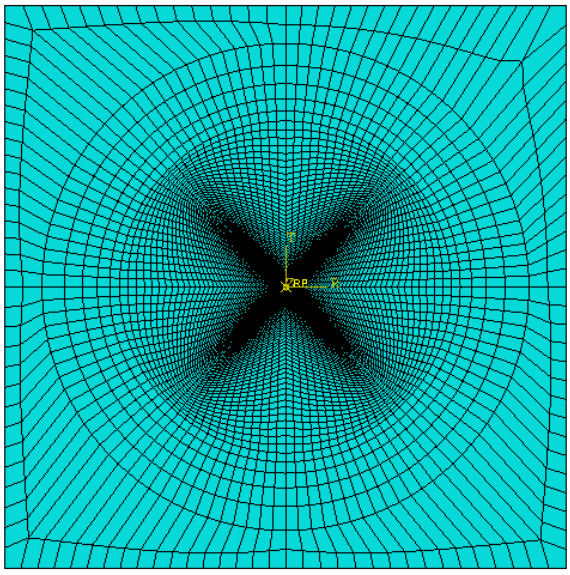

Figure 3.1: Mesh on a PC plate (top view).

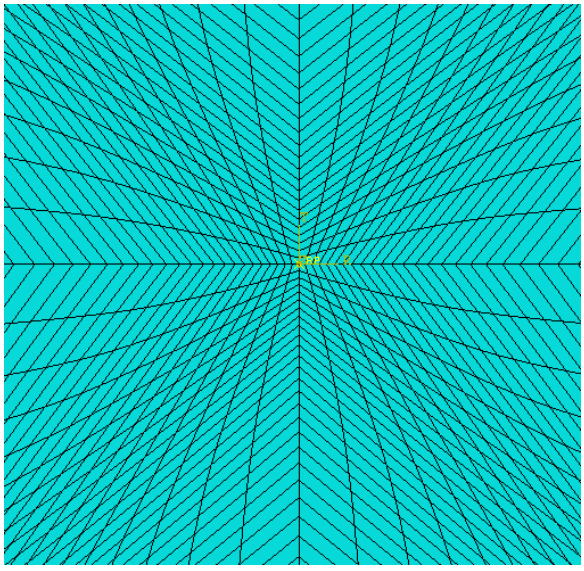

Figure 3.2: Mesh on a PC plate (enlarged top view).

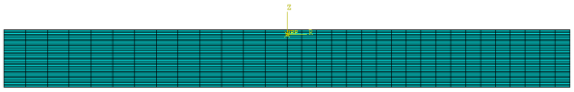

Figure 3.3: Mesh on a PC plate (side view).

Fixed boundary condition is used in the top and bottom clamped area for the target plate. Figure 3.6 shows the bottom boundary conditions. The top boundary condition is also same.

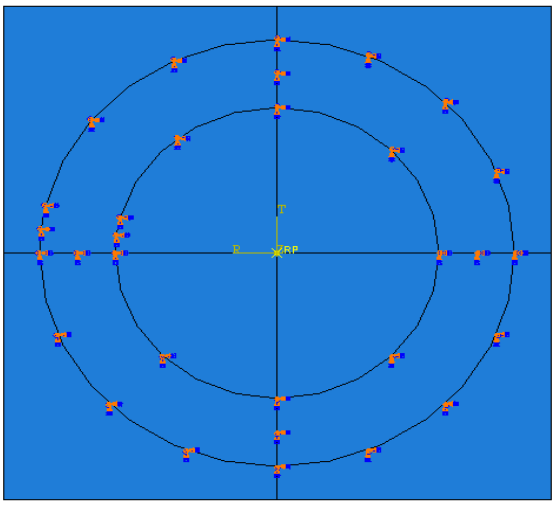

Figure 3.4: Boundary Condition at Bottom Face.

3.2.1 Modeling of the Striker

Figure 3.5 shows the striker which is made of steel. Instead of whole striker, only the striker tip was modeled since striker was modeled as 3D discrete rigid body. Figure 3.6 shows the modeled striker tip. A rigid body constraint was used for the striker with point mass/inertia engineering features. The mass of the actual striker was assigned to the reference point of the modeled striker. Figure 3.8 shows enlarged view of the mesh on the striker. The striker was modeled using R3D4 elements which are 3D quadrilateral discrete rigid elements.

Figure 3.5: Actual Striker Tip.

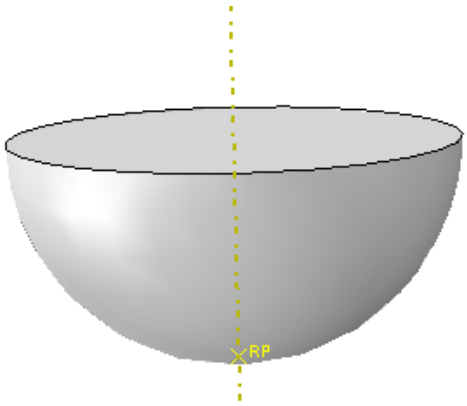

Figure 3.6: Modeled Striker Tip.

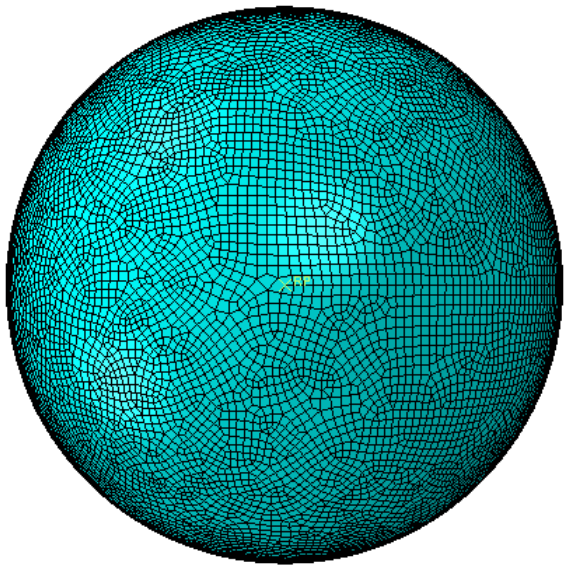

Figure 3.7: Enlarged view of mesh on the striker.

A displacement/rotation boundary condition was used to restrict the motion of striker. In actual experiment the striker can move only in the z-direction. This condition was applied to the striker so that it will move only in the z-direction, and all other degrees of freedom are constrained.

In the experiment the input parameter was the impact energy of the striker. The striker was originally positioned very close to the target plate with an initial velocity (which is equal to the required velocity for the corresponding impact energy of the experiment).

In this model impact only within the elastic limit of the material was considered i.e. no plastic deformation or damage was not considered here. The maximum impact force and contact duration was taken from the simulation to compare with the experimental results.

Chapter 4: Results and Discussions

4.1 Failure of a single PMMA plate

Impact experiments were carried out on a single PMMA plate of dimension 127×127×11.5 mm^3 to see the damage pattern. To find the critical energy at which a single PMMA plate would fail, impact energies were gradually increased starting from 1J until damage was seen. Damage is defined by plastic deformation or initial crack. Figure 4.1 shows the top view of the PMMA plate at 11J energy. A theoretical prediction was made for maximum contact force and contact duration using equation 3.8 and 3.9. Figure 4.2 and 4.3 shows the variation of maximum impact force and contact duration with respect to impact energy. Figure 4.2 shows the theoretical value with the simulated value. This values are very close to each other but the experimental value for very low energy impact is close to the theoretical and simulated value. For higher energy impacts, the experimental values differ from the theoretical and simulated values more, the reason of this variation is because the theory is applicable only within the elastic limit and the simulation was carried out without any inelastic constitutive models, but in the experiment there is some plastic deformation as well as softening from the cumulative damage. Another reason is the bending effect. In theory, it was assumed that the target plate is thick enough to resist bending (assumption of equation 3.8) but due to a larger mass of the striker there might be bending which is not negligible. For plastic deformation, all the kinetic energy of the projectile is not used in the contact but some energy is used to deform the material plastically. This is also applicable to simulation since simulation was also carried out for elastic deformation. The post mortem analysis of impact damage on a single PMMA plate shows that the crack initiates not in the point of impact, rather it initiates from the bottom face of the target plate. Illustration 4.1 shows the exact location from where the crack initiates. This is due to the fact that in this case the failure mechanism is flexural wave dominated because of the large mass ratio of the projectile and target plate as discussed in section 1.2.2.

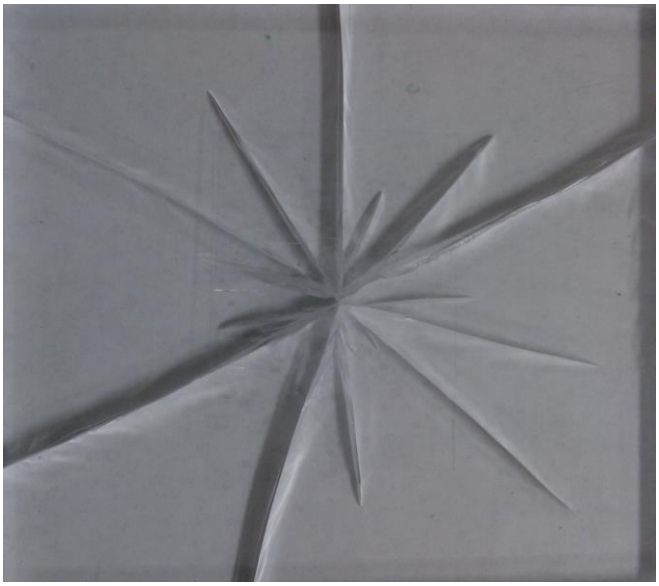

Figure 4.1: Top view of Damaged Single PMMA Plate.

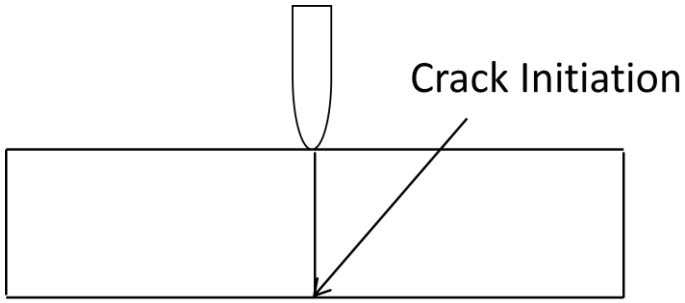

Illustration 4.1: Location from where crack initiates.

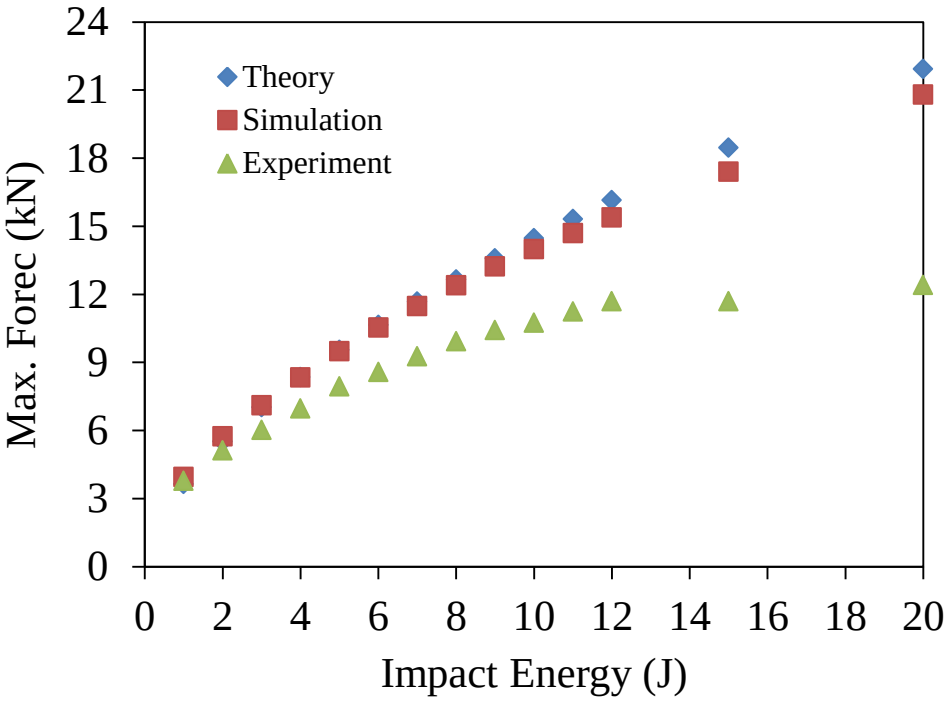

Figure 4.2: Variation of Maximum Impact Force with Energy for Single PMMA Plate.

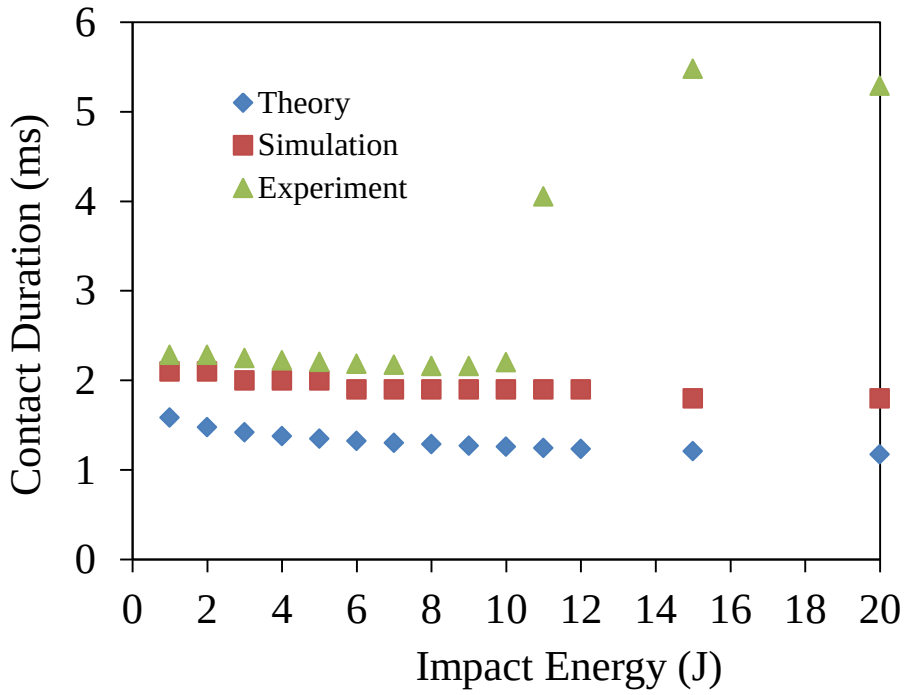

Figure 4.3: Variation of Contact Duration with Energy for Single PMMA Plate.

Figure 4.3 shows the theory slightly under predicts the contact duration both from simulation and experiment. For impact energy up to 11J the trend for both three curves (theory, simulation and experiment) is same but at 11J energy the experimental value of contact duration suddenly increases, this is because at this energy the plate fails i.e. crack initiates and propagates so the striker stays in contact with the plate for a comparatively longer period of time.

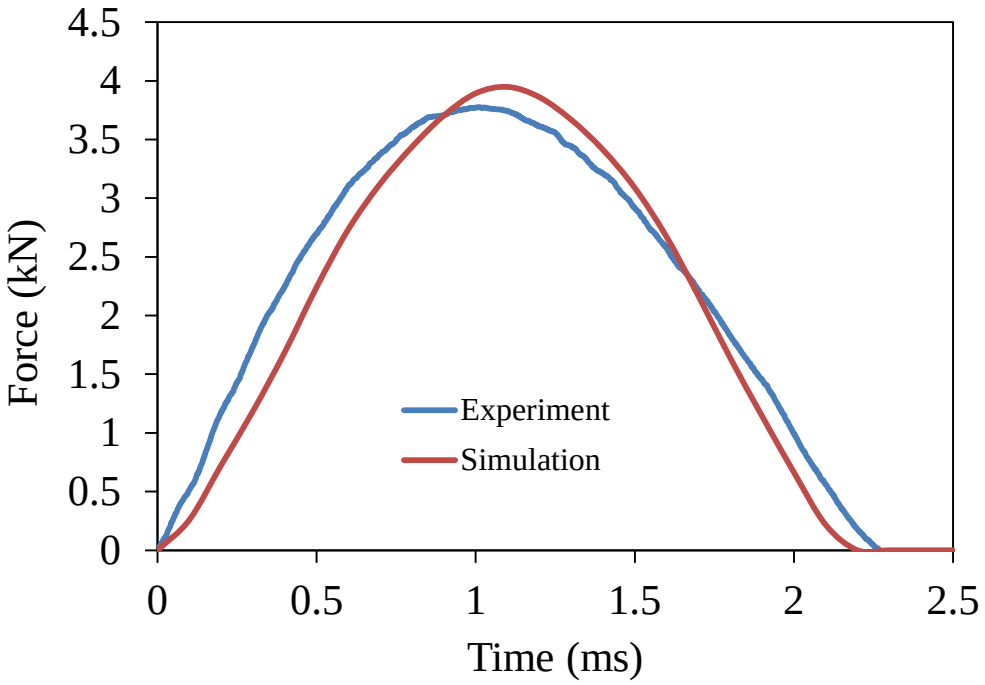

Figure 4.4: Impact Force VS Time for 1J Energy.

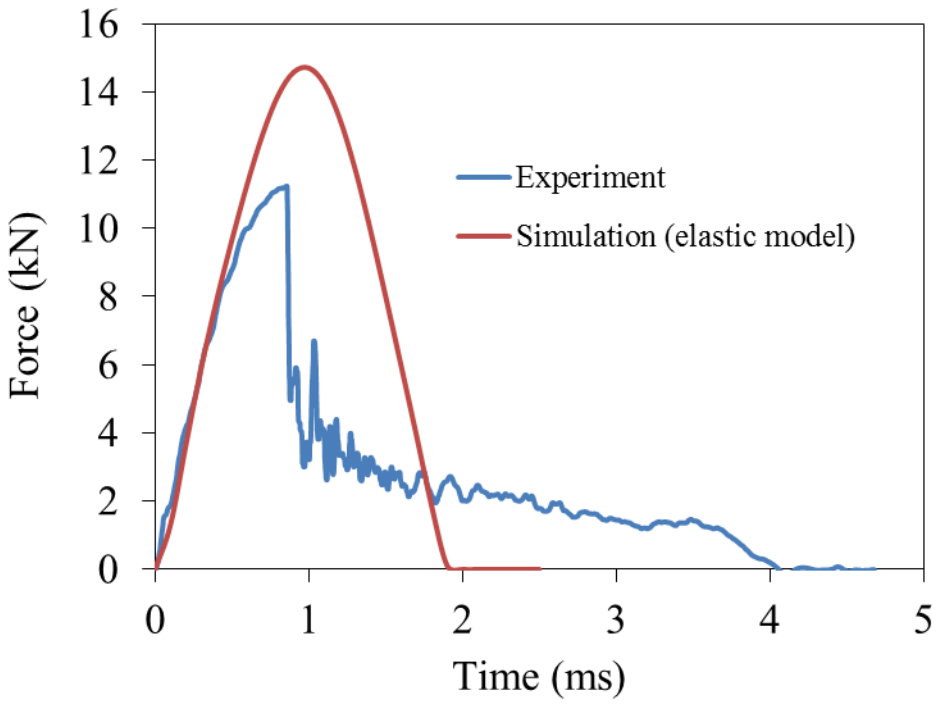

Figure 4.5: Impact Force VS Time for 11J Energy.

Figure 4.4 and 4.5 shows the impact force time history for 1J and 11J impact energy respectively from both experiment and simulation. For very low energy impact energy (figure 4.4), the force-time history is almost identical both from simulation and experiment but as the impact energy increases, the variation between these two also increases. The reason for variation in the maximum contact force is discussed earlier. Table 4.1 shows the values of maximum impact force and contact duration for single PMMA specimen.

Table 4.1: Maximum Impact Force and Contact Duration for Single PMMA Specimen.

Material: PM.5						
	Force(kN)			Contact Duration (ms)		
Energy(J)	Theoretical	Simulation	Experimental	Theoretical	Simulation	Experimental
1	3.63475	3.94834	3.776	1.5842	2.1	2.286
2	5.50926	5.74217	5.113	1.4781	2.1	2.284
3	7.02664	7.10887	6.026	1.4194	2.0	2.249
4	8.35047	8.33604	6.971	1.3792	2.0	2.225
5	9.54678	9.48542	7.936	1.3487	2.0	2.207
6	10.6504	10.5357	8.573	1.3244	1.9	2.184
7	11.6824	11.4845	9.261	1.3041	1.9	2.1725
8	12.6569	12.3981	9.923	1.2868	1.9	2.161
9	13.5838	13.2243	10.427	1.2717	1.9	2.159
10	14.4702	13.9845	10.741	1.2584	1.9	2.202
11	15.3218	14.7023	11.240	1.2465	1.9	4.055
12	16.1430	15.3858	11.693	1.2357	1.9	4.78
15	18.4557	17.197	11.691	1.2084	1.8	5.48
20	21.9327	19.831	12.417	1.1741	1.8	5.291

4.2 IMPACT ON A SINGLE POLYCARBONATE PLATE

To get the maximum impact force and contact duration on a single polycarbonate (PC) plate both these three approach were used namely, theory (equation 3.8), simulation and experiment. Figure 4.6 shows the maximum impact force vs impact energy for a single PC plate. It is shown that for low energy impact energy, the maximum force at low energy in all the three approaches are very close but at higher energy level, the theoretical and simulation value are very close to each other and while the experimental value is much lower than the two. One of reason for this variation might be the plastic deformation on the impact site. On the impact site it was seen some plastic deformation, so all the kinetic energy of the projectile was not used in the contact but some energy goes to deform the material plastically. Another reason might be the assumption on the theory because equation 3.8 only in case of very little or no bending of the specimen during the impact. But in case of high energy impact there was some bending on the specimen.

Figure 4.7 shows the variation of contact duration with respect to impact energy. It shows that the theory greatly under predicts the contact duration. The simulated value is somewhat in the middle

between experimental value and the theoretical value. Figure 4.8 shows the plastic deformation on a PC plate. The impact machine was a low velocity high energy type impact machine for this reason we can't increase the striker velocity beyond a certain limit although we can increase the impact energy by increasing the striker mass. The PC specimen cannot break at low velocity impact, it only deform plastically because, Polycarbonate is very tough and high impact resistance over other polymers (PMMA) [19-33]. Table 4.2 shows the values of maximum impact force and contact duration for single PC specimen.

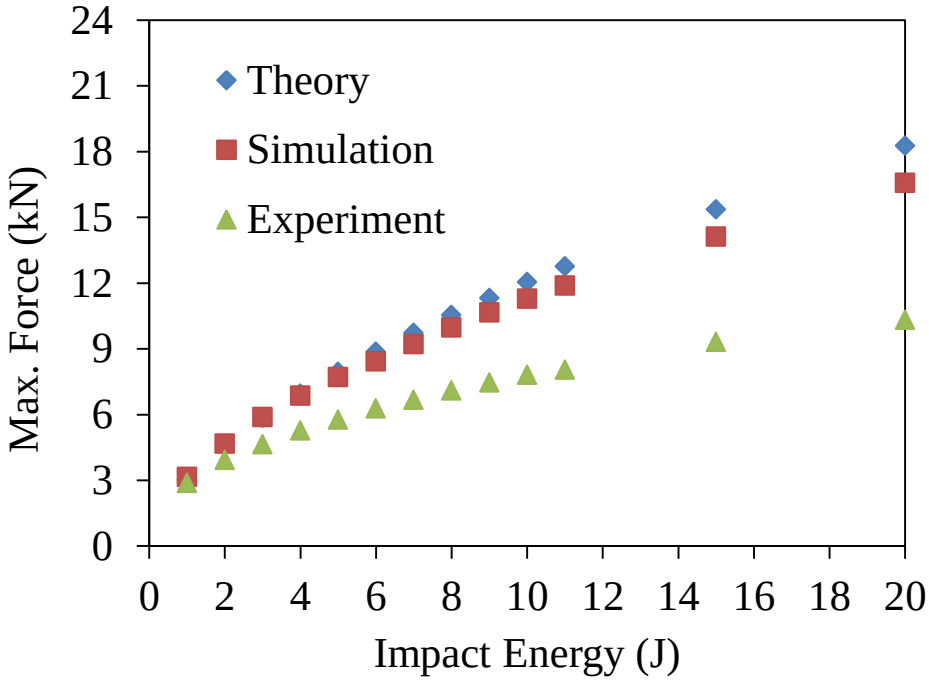

Figure 4.6: Variation of Maximum Impact Force with Impact Energy for PC.

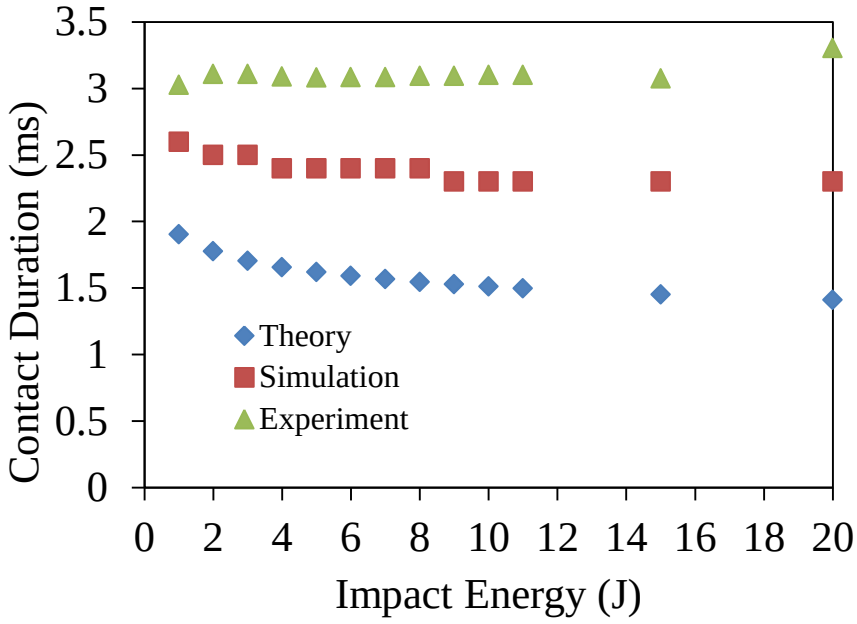

Figure 4.7: Variation of Contact Duration with Impact Energy for PC.

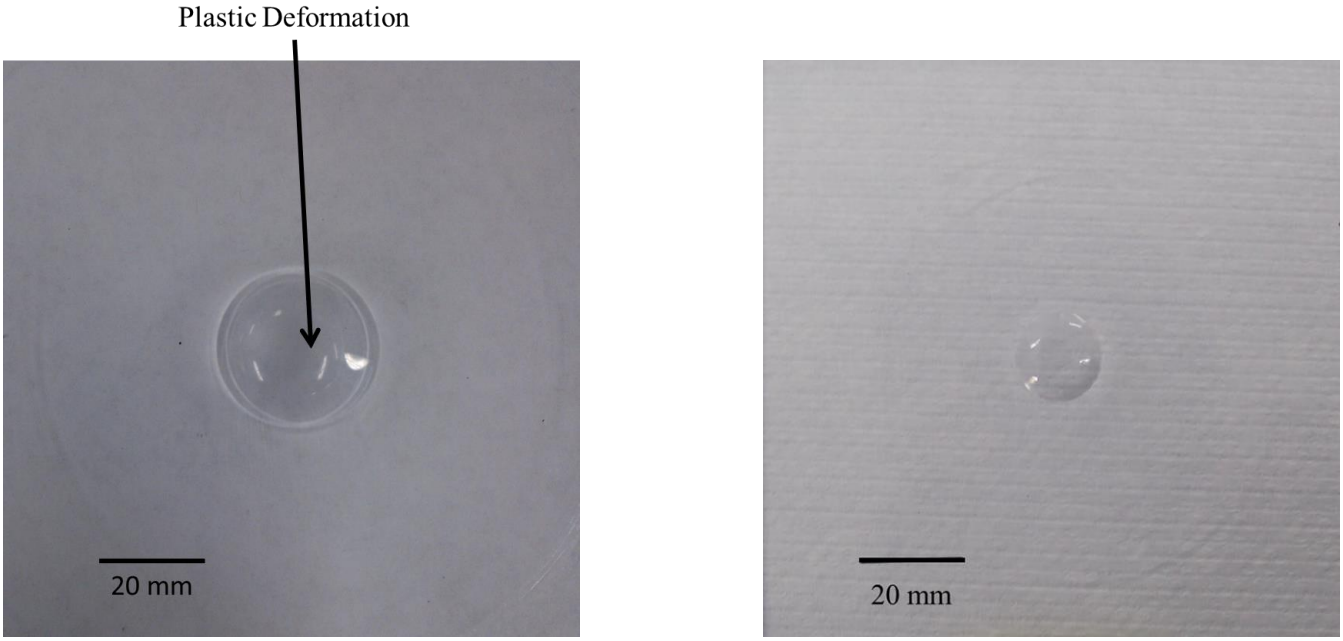

(a) (b)

Figure 4.8: Plastic Deformation on a PC Plate (a) Top View and (b) Bottom View.

Table 4.2: Maximum Impact Force and Contact Duration for Single PC Specimen.

Material: PC.5						
	Force(kN)			Contact Duration (ms)		
Energy(J)	Theoretical	Simulation	Experimental	Theoretical	Simulation	Experimental
1	3.02636	3.14774	2.874	1.9027	2.6	3.0263
2	4.58710	4.66764	3.924	1.7753	2.5	3.1088
3	5.85051	5.87991	4.642	1.7048	2.5	3.1088
4	6.95275	6.86159	5.264	1.6564	2.4	3.0886
5	7.94882	7.70451	5.763	1.6199	2.4	3.0826
6	8.86771	8.42740	6.28	1.5906	2.4	3.085
7	9.72701	9.21901	6.677	1.5663	2.4	3.085
8	10.5384	9.97441	7.099	1.5455	2.4	3.0938
9	11.3101	10.6624	7.459	1.5274	2.3	3.095
10	12.0482	11.2842	7.806	1.5114	2.3	3.1025
11	12.7572	11.8789	8.041	1.4970	2.3	3.2603
15	15.3665	14.1195	9.322	1.4513	2.3	3.075
20	18.2616	16.5675	10.32	1.4102	2.3	3.3025

4.3 IMPACT ON LAYERED SPECIMEN

A series of impact experiments were carried out on different layered specimens. Figure 4.9 and table 4.3 shows the variation of maximum impact force with respect to impact energy for both single and layered specimen of equal thickness. It shows that for single specimen, the maximum impact force increases with increasing impact energy up to 11 J but after 11 J it is almost constant. The reason for this is due to the fact that a single PMMA specimen fails at this energy and if we increase the impact energy, the additional energy is used to damage the material. For layered specimen, after 5 J energy the force doesn't increase with energy because the top plate fails at this energy and the additional energy is used to further damage the specimen.

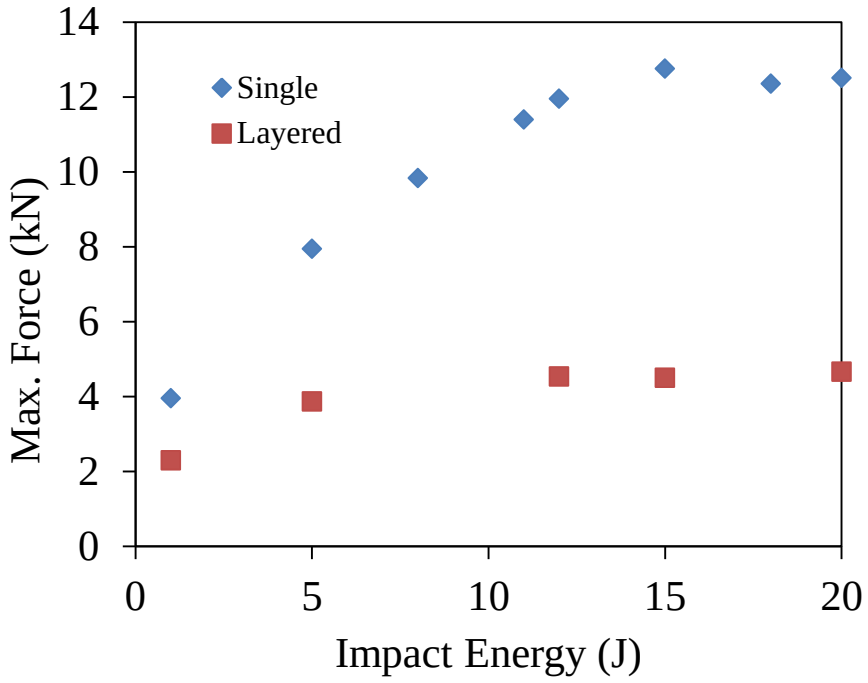

Figure 4.9: Variation of Maximum Force for both Single and Layered PMMA Specimen.

Table 4.3: Maximum Impact Force for Single and Layered PMMA Specimen.

Specimen: PM.5	
Impact Energy (J)	Max. Force (kN)
1	3.953
5	7.943
8	9.83
11	11.394
12	11.953
15	12.753
18	12.352
20	12.505
Specimen: PM.25/.25	
1	2.296
5	3.87
12	4.536
15	4.499
20	4.662

Figure 4.10 shows the top and bottom plate of a specimen of two equal thickness PMMA plate at 6J impact energy. These figures show that the crack on the top plate can't penetrate to the bottom plate.

After impact post mortem shows that the crack actually starts from the bottom of the top plate and then propagates three dimensionally on the top plate only and the bottom plate remain intact. The crack initiation location is sketched on illustration 4.2. The reason for this might be the effect of adhesive, so that during impact the adhesive just below the impact location compressed significantly to allow the top plate to bend (thus the top plate fails) but the energy level is not sufficient to bend the bottom plate, this situation is sketched on illustration 4.3.

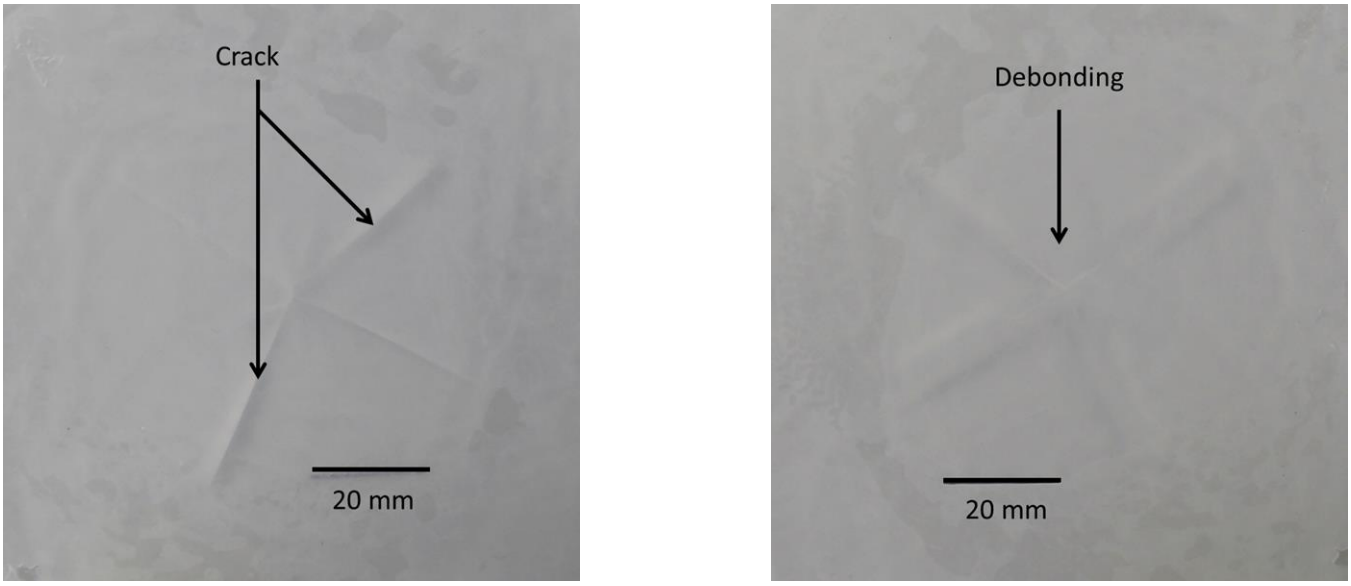

(a) (b)

Figure 4.10: Layered PMMA Specimen at 6J Energy (a) Top Plate and (b) Bottom Plate.

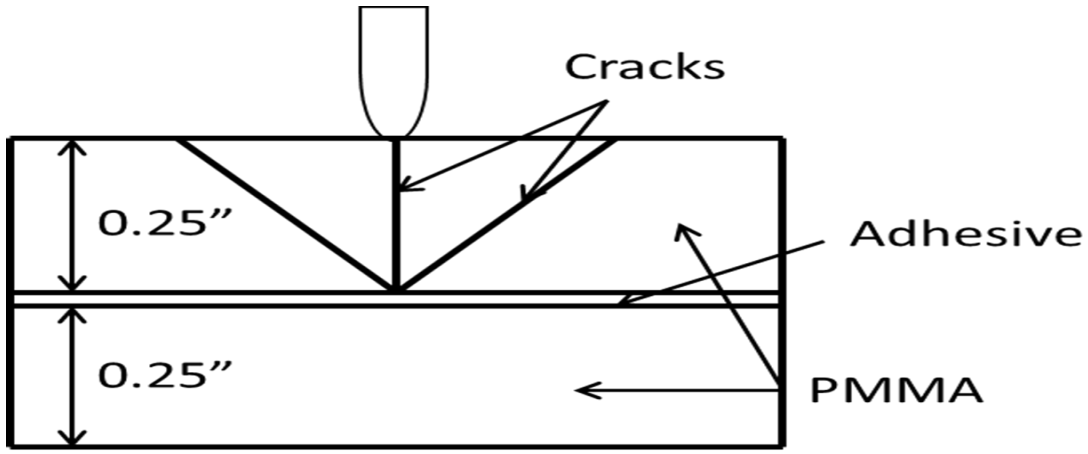

Illustration 4.2: Location from where crack initiates for layered specimen.

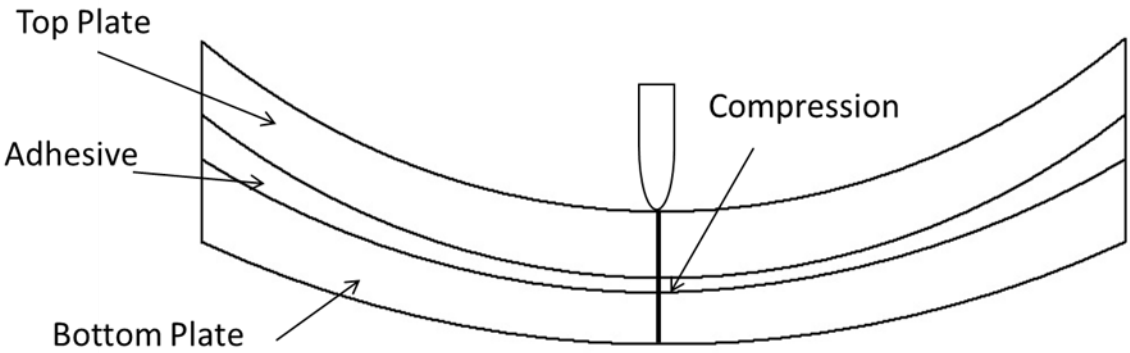

Illustration 4.3: Compression in the adhesive layer.

To confirm this phenomenon that the adhesive layer is playing an important role on the damage of the top layer but bottom layer remains intact, impact test were carried out on a single plate of layered specimen and it was found that the single plate damaged only at 2J energy (Figure 4.11). Another experiment was carried on a layered specimen at 6J impact energy but without any adhesive and it was found that at this energy both plate damaged. For the layered specimen (with adhesive) at 6J energy, only the top plate fails but for layered specimen (without adhesive) both plate fails. So, the adhesive layer is playing an important role on the damage mechanism. Figure 4.12 shows the top and bottom plate of damaged layered specimen without adhesive.

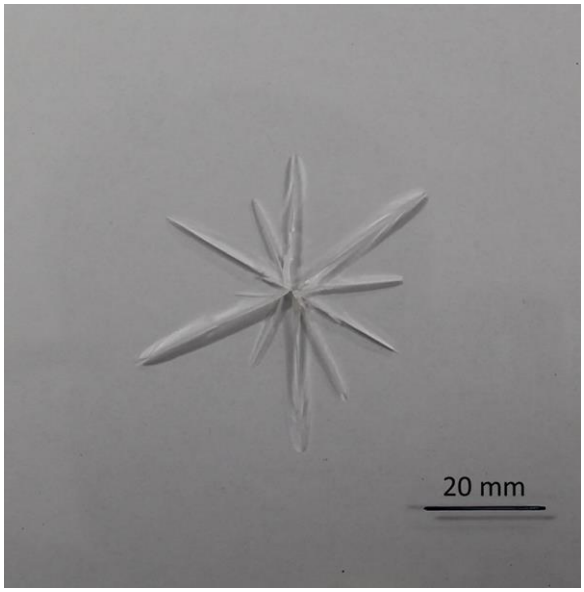

Figure 4.11: Damaged PMMA Plate at 2J Energy.

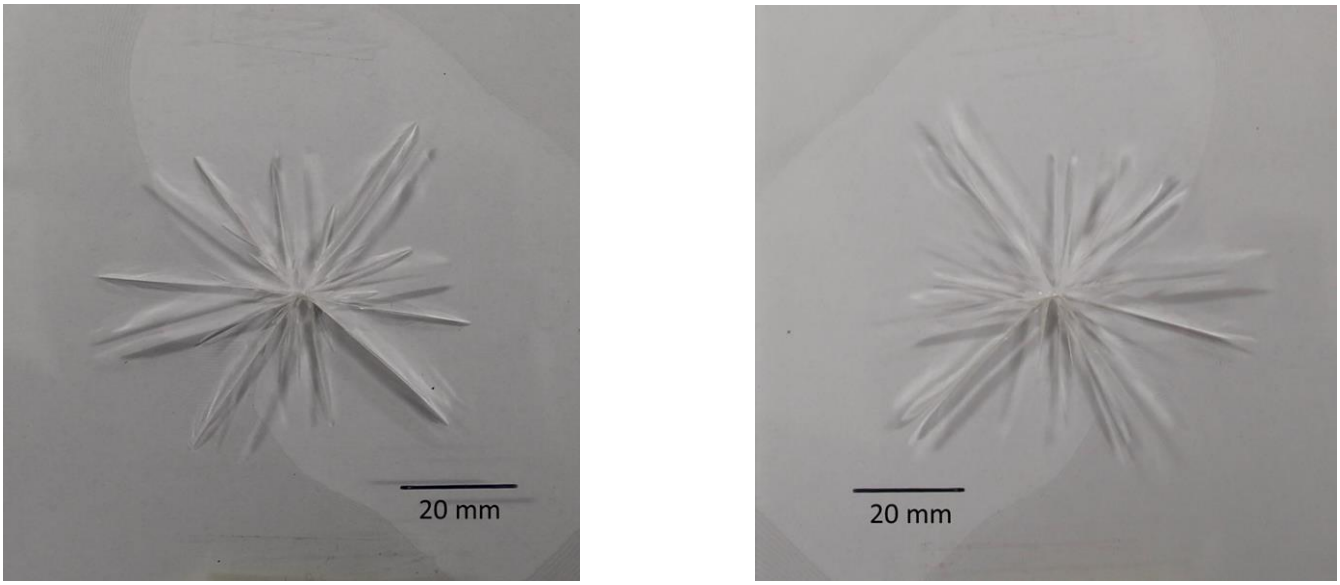

(a) (b)

Figure 4.12: Layered PMMA Specimen (without adhesive), (a) Top Plate and (b) Bottom Plate.

When the impact energy is comparatively higher (20J), then both top and bottom plate of the layered specimen fails but doesn't shatter. Figure 4.13 shows the top and bottom plate of the layered specimen at 20J impact energy. But in case of a single specimen of same thickness, the specimen fails and the material at the impact zone shatter which creates a hole of diameter about 10 mm on the top side and 20 mm on the bottom side. Figure 4.14 shows the top and bottom view of the damaged specimen.

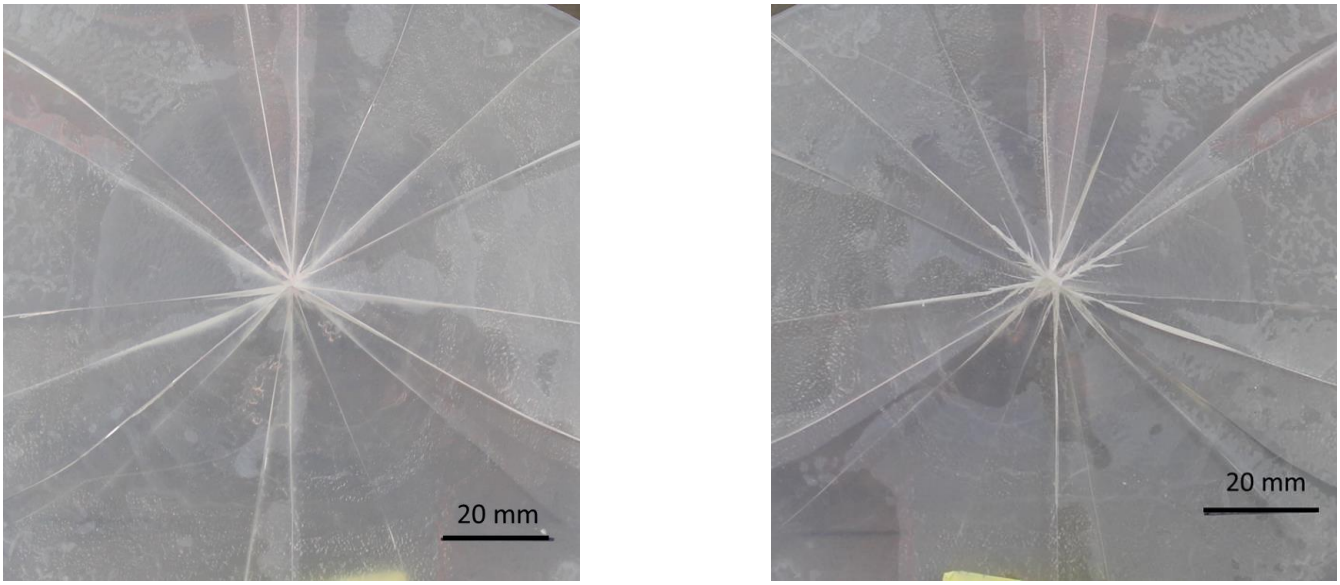

(a) (b)

Figure 4.13: Layered PMMA Specimen at 20J Impact Energy (a) Top Layer and (b) Bottom Layer.

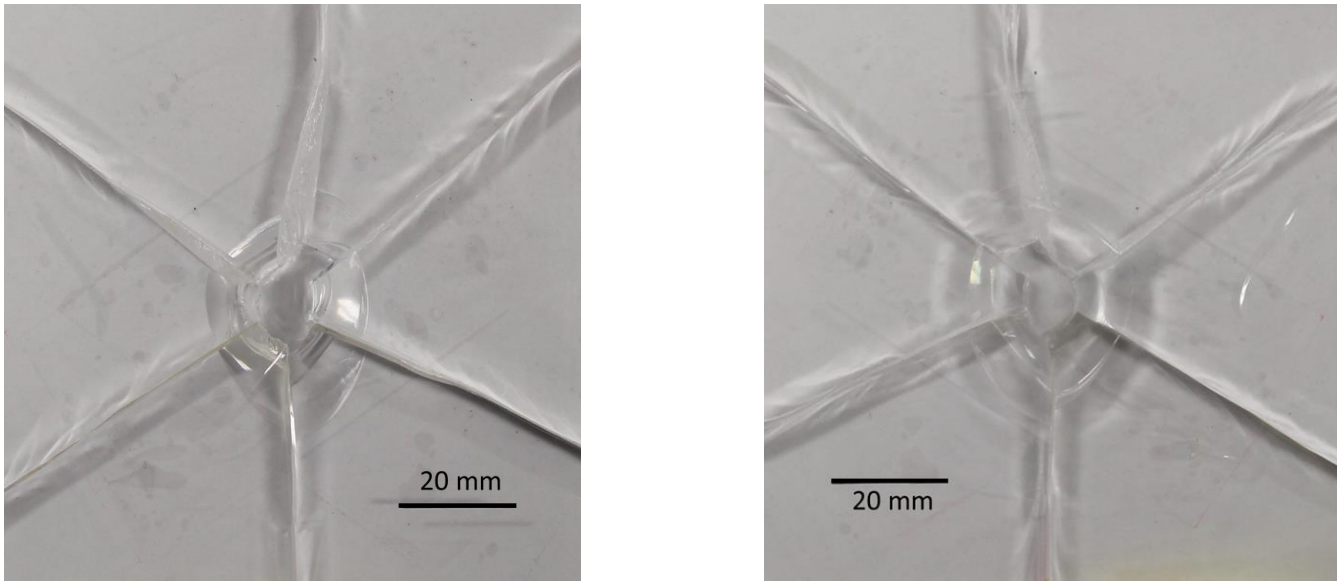

(a) (b)

Figure 4.14: Single PMMA Specimen at 20J Impact Energy (a) Top View and (b) Bottom View.

Figure 4.15 shows the top and bottom view of a layered PC specimen at 120J energy impact. It shows that plastic deformation on the top layer but almost no effect on the bottom layer. Figure 4.16 shows the variation of maximum impact force with respect to energy for both single and layered PC specimen of equal thickness. This shows that the maximum force is much smaller for layered specimen. Table 4.4 shows the maximum impact force both for single and layered PC specimen.

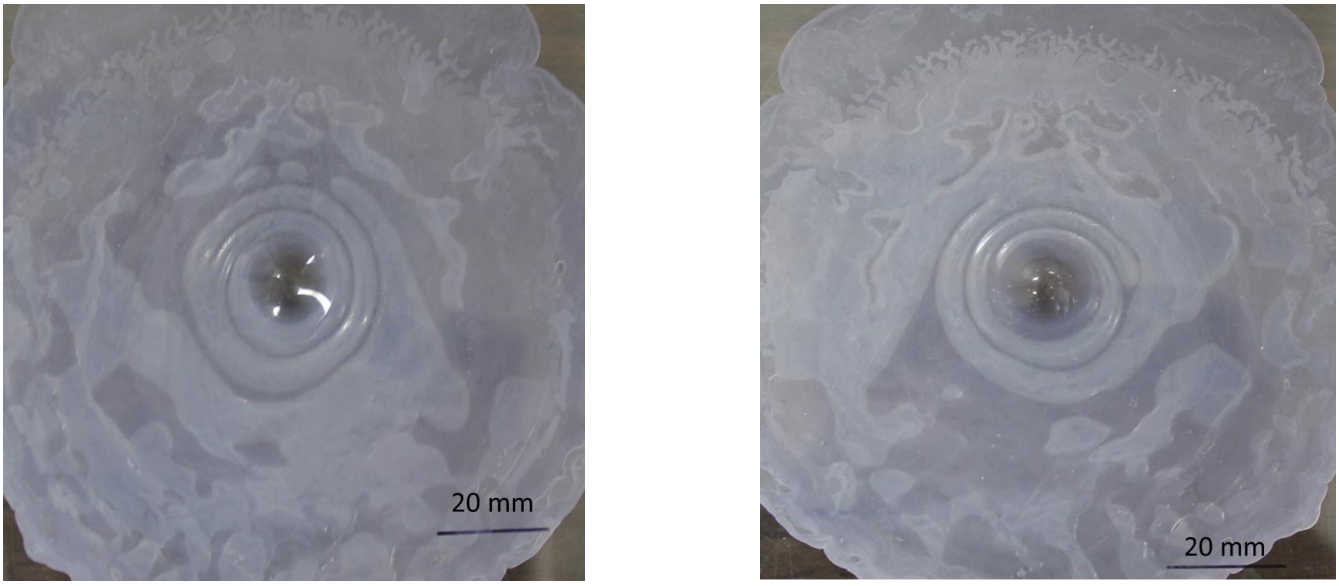

(a) (b)

Figure 4.15: Layered PC Specimen at 120J Energy (a) Top View and (b) Bottom View.

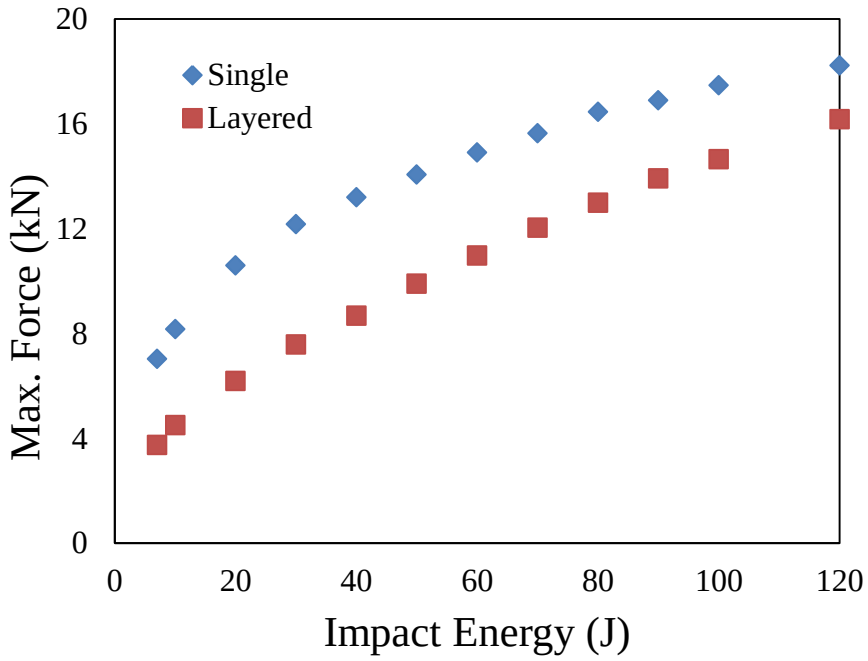

Figure 4.16: Maximum Impact Force VS Impact Energy for Single and Layered PC.

Table 4.4: Maximum Impact Force for Single and layered PC Specimen.

	Specimen	
	PC.5	PC.25/.25
Impact Energy (J)	Max. Force (kN)	Max. Force (kN)
7	7.034	3.751
10	8.161	4.497
20	10.59	6.191
30	12.169	7.575
40	13.196	8.681
50	14.058	9.903
60	14.901	10.972
70	15.639	12.035
80	16.448	12.99
90	16.886	13.913
100	17.462	14.648
120	18.218	16.175

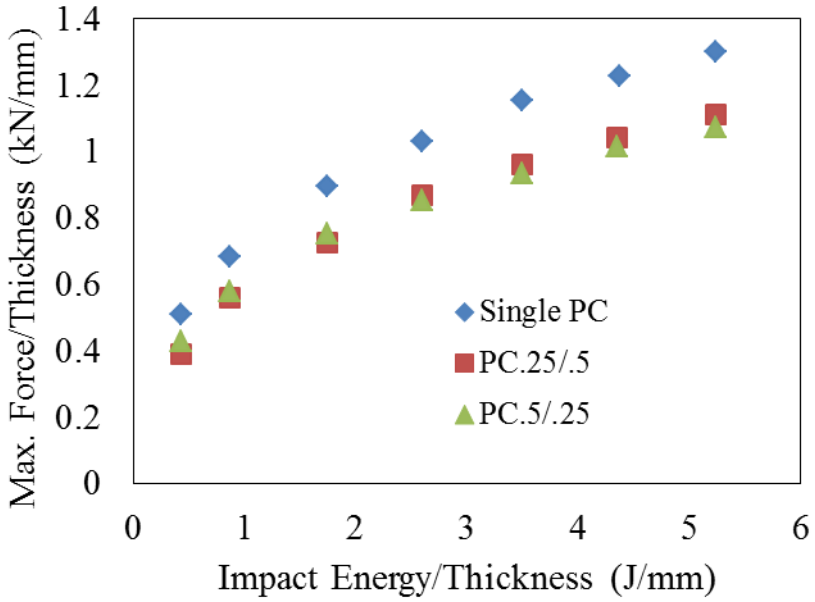

Figure 4.17: Maximum Impact Force VS Impact Energy for Single and Layered PC.

Table 4.5: Maximum Impact Force for Single and layered PC Specimen (different thickness).

Specimen: PC.5			
Impact Energy (J)	Energy/Thickness	Max.Force(kN)	Max. Force/thick. (kN/mm)
5	0.434027778	5.848	0.507638889
10	0.871839582	7.821	0.681865737
20	1.743679163	10.279	0.896163906
30	2.59965338	11.878	1.029289428
40	3.493449782	13.196	1.152489083
50	4.366812227	14.058	1.227772926
60	5.235602094	14.901	1.30026178
Specimen: PC.25/.5			
7.6384	0.434	6.872	0.390454545
15.19895	0.871	9.754	0.558968481
31.20016	1.744	12.976	0.725321409
45.942	2.6	15.341	0.86819468
61.86103	3.493	17.041	0.962224732
77.31534	4.346	18.503	1.040078696
92.36304	5.236	19.638	1.113265306
Specimen: PC.5/.25			
7.7035	0.434	7.564	0.426140845
15.43412	0.871	10.237	0.577708804
30.74672	1.744	13.263	0.752297221
45.812	2.6	15.024	0.852667423
61.61652	3.493	16.504	0.935600907
76.79382	4.346	17.962	1.016525184
92.72956	5.236	18.973	1.071315641

Figure 4.17 is also for single and layered PC specimen but in this case the thickness of single plate is about 0.5” and the thickness of layered specimen is 0.75” (0.25”+0.5”), in order to compare the result for this two, the impact force per unit thickness with respect to impact energy per unit thickness was considered. In this figure, the legend PC .25/.5 indicates that for layered specimen impact on .25” PC plate and PC.5/.25 indicates that impact on 0.5” PC plate. This figure shows that the maximum force for PC.25/.5 and PC.5/.25 is almost same which is slightly less from single PC specimen. For both these

cases there was only a little plastic deformation on the impacted plate but the other plate was intact. Table 4.5 shows these results in tabular form.

Figure 4.18 and table 4.6 shows the variation of maximum force with impact energy for bi-material layered specimen, single PC and PMMA specimen of equal thickness. In this figure the legend PM.25/PC.25 and PC.25/PM.25 indicates that impact was done on PMMA and PC plate respectively. This shows that for layered material, the maximum force is much smaller than the single specimen. In this case always the PMMA plate fails irrespective on which plate impact was done i.e. when impact was on PMMA plate then PMMA plate fails but when impact on PC plate, still the PMMA (bottom) plate fails. Figure 4.19 and 4.20 shows the failure on bi-material at 20J energy when impact on PMMA and PC plate respectively.

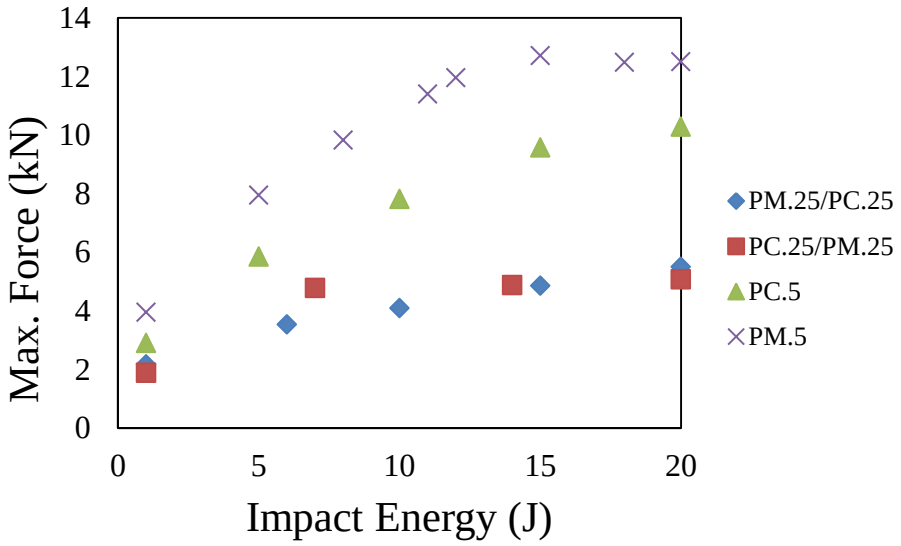

Figure 4.18: Maximum Impact Force VS Impact Energy for Bi-material.

Table 4.6: Maximum Impact Force for Bimaterial

Specimen: PM.25/PC.25	
Impact Energy (J)	Max. Force (kN)
1	2.176
6	3.536
10	4.092
15	4.857
20	5.499
Specimen: PC.25/PM.25	
1	1.885
7	4.782
14	4.883
20	5.076

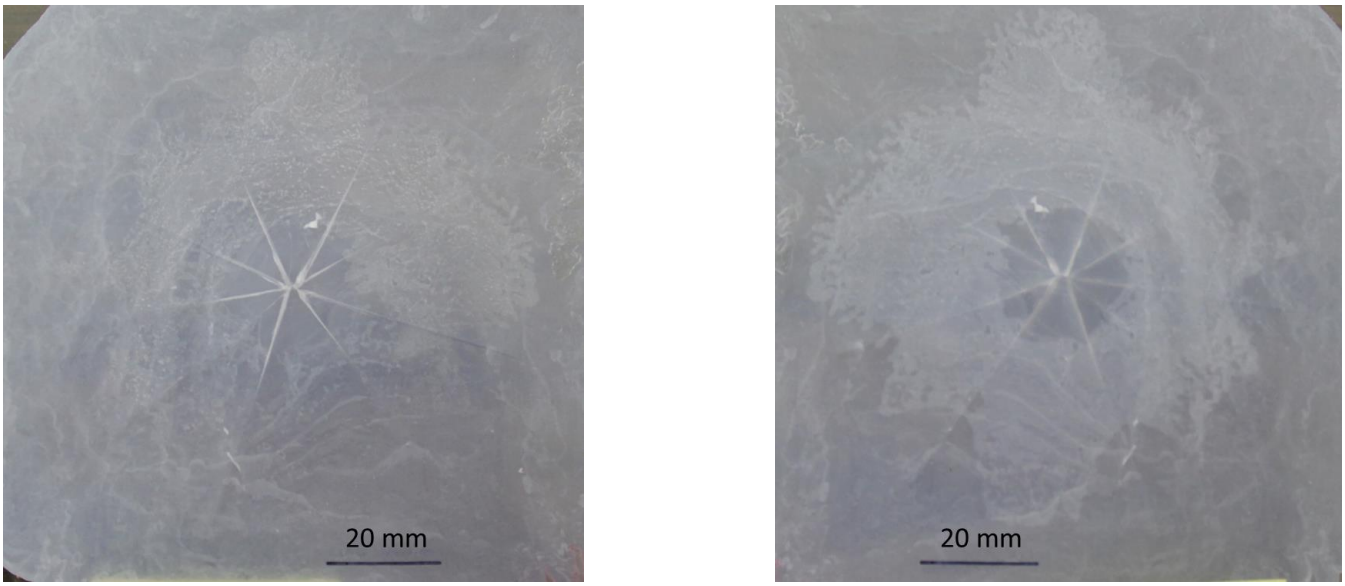

(a) (b)

Figure 4.19: Layered Bi-material Specimen at 20J Impact Energy (a) Top Layer (PMMA) and (b) Bottom Layer (PC).

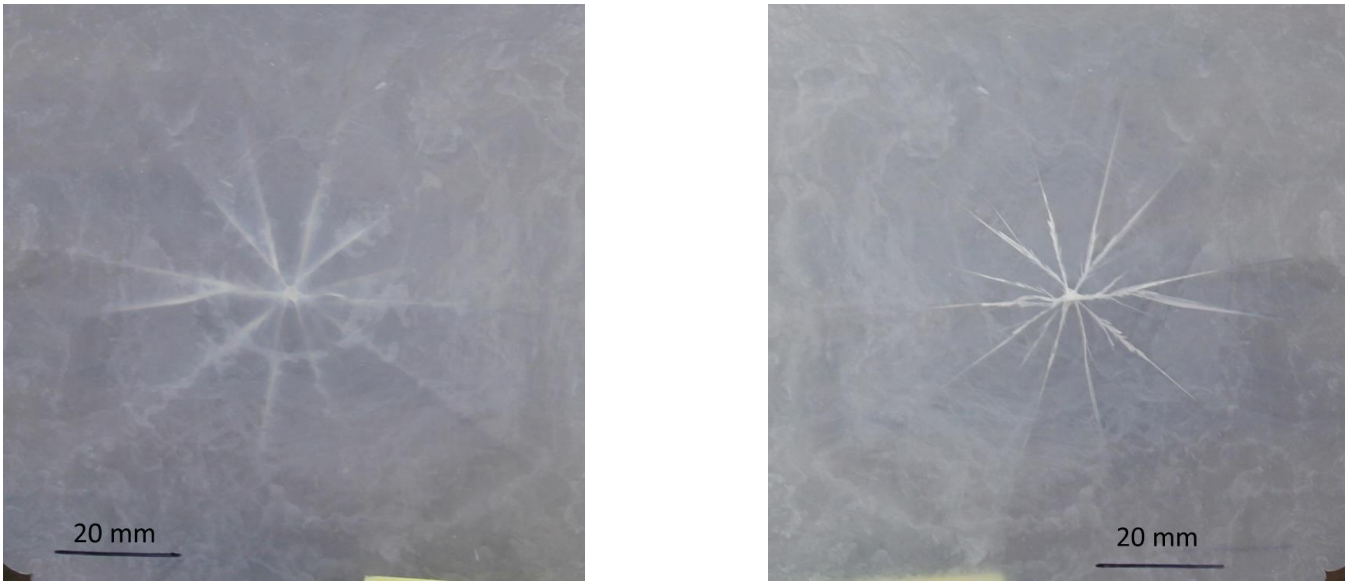

(a) (b)

Figure 4.20: Layered Bi-material Specimen at 20J Impact Energy (a) Top Layer (PC) and (b) Bottom Layer (PMMA).

Chapter 5: Analytical Solution

In order to find an analytical solution, it was assumed that the top and bottom layer can bend independently, i.e. their deflection is not same. The deflection was expressed in terms of Fourier series as shown in equation 5.1 and 5.2.

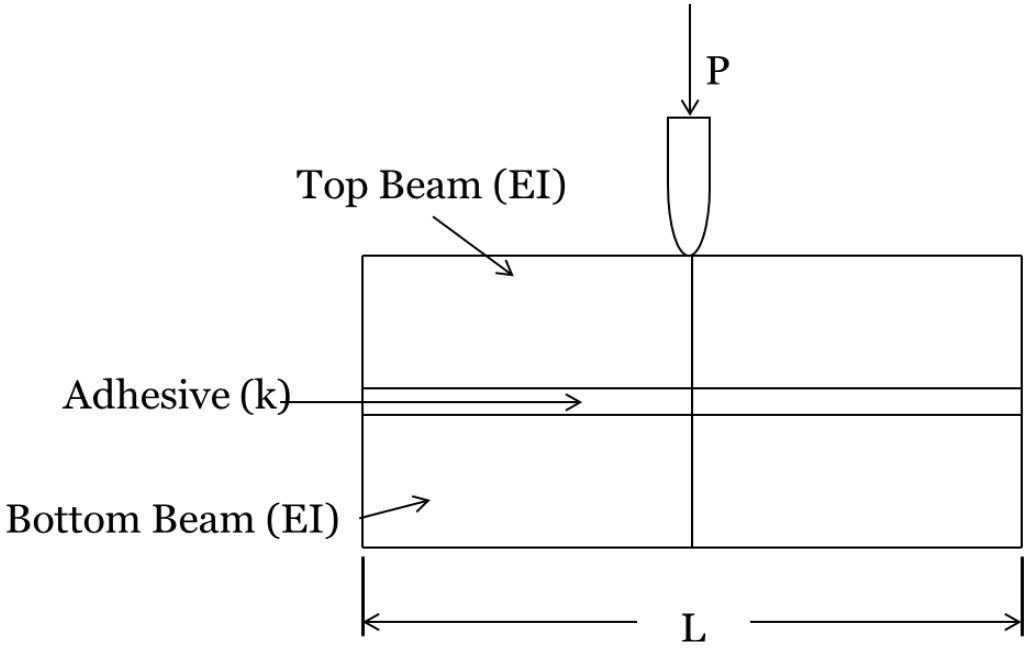

Illustration 5.1: Different parameters used in analysis.

Deflection on upper beam,

$$W_u = A\left[\mathrm{Cos}\left(\frac{2\pi x}{L}\right) + 1\right] \qquad (5.1)$$

Deflection on lower beam,

$$W_l = B\left[\mathrm{Cos}\left(\frac{2\pi x}{L}\right) + 1\right] \qquad (5.2)$$

Where A and B are constants.

The energy used during impact on the upper and lower beam can be expressed as,

$$U_u = \int_{-L/2}^{L/2} \frac{EI}{2} (W_u'')^2 dx \qquad (5.3)$$

$$U_l = \int_{-L/2}^{L/2} \frac{EI}{2} (W_l'')^2 dx \qquad (5.4)$$

Deflection on adhesive layer can be expressed as the difference between the deflection of upper and lower beam,

$$\delta = W_u - W_l \qquad (5.5)$$

So the energy absorbed by the adhesive layer,

$$U_g = \int_{-L/2}^{L/2} \frac{k}{2}(\delta)^2 dx \qquad (5.6)$$

External work done by the applied quasi-static force,

$$W_{ext}=P*W_u[0] \qquad (5.6)$$

So, the total energy of the system is the sum of energy that goes to the upper beam, to the lower beam, to the adhesive layer minus the external work done by the applied force,

$$E=U_u+U_l+U_g-W_{ext} \qquad (5.7)$$

To minimize the total energy, Rayleigh-Ritz method was used, i.e. differentiation of equation 5.7 with respect to A and B was taken the equations were solved for A and B. Then the value of the coefficients A and B was putted back to equations 5.1 and 5.2 to find the expression of the deflections. Then the value of U_u, U_l, U_g and W_{ext} were found. Then the ratio of the energy that goes to the lower beam to the external work after simplifying can be expressed as,

$$\frac{U_l}{W_{ext}} = \frac{9k^2L^8}{4(3kL^4 + 8EI\pi^4)(3kL^4 + 16EI\pi^4)}$$

By considering unit value of these parameters, i.e.

L=1, E=1, I=1, we get,

$$\frac{U_l}{W_{ext}} = \frac{9k^2}{4(3k+8\pi^4)(3k+16\pi^4)} \qquad (5.8)$$

Now, stress on upper and lower plate,

$$\sigma_u = \frac{Mc}{I} \text{ Where, } M = EIW_u''$$

By simplifying,

$$\sigma_u = W_u'' \qquad (5.9)$$

Similarly for lower plate,

$$\sigma_u = W_l'' \qquad (5.10)$$

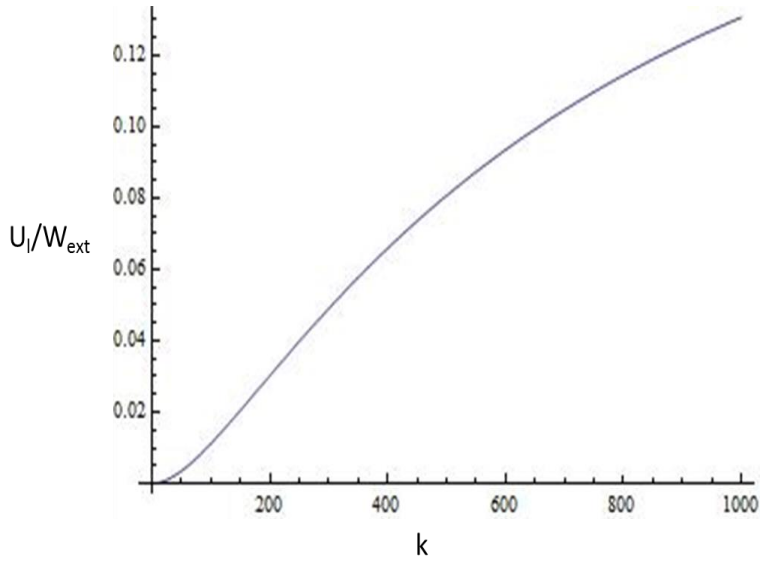

Figure 5.1: Variation of U_l/W_{ext} with respect to k (equation 8).

Figure 5.1 shows the variation of $\frac{U_l}{W_{ext}}$ as a function of k and it shows that when the value of k increases, $\frac{U_l}{W_{ext}}$ also increases. This is because, if the value of k tends to the stiffness of the material used then there will be no effect of layer i.e. the layered specimen will act like a single material. Figure 5.2 and 5.3 shows the deflection on top and bottom layer respectively. The deflection on the top layer is much more than that of bottom layer. This implies that the adhesive layer absorbs some of the impact energy so all the energy doesn't transmit to the bottom layer and that's why the deflection on the bottom layer is much smaller than the top layer. Figure 5.4 and 5.5 shows the variation of flexural stress on the top and bottom layer respectively. The stress on the top layer is much more than the bottom layer because the deflection on the top layer is more.

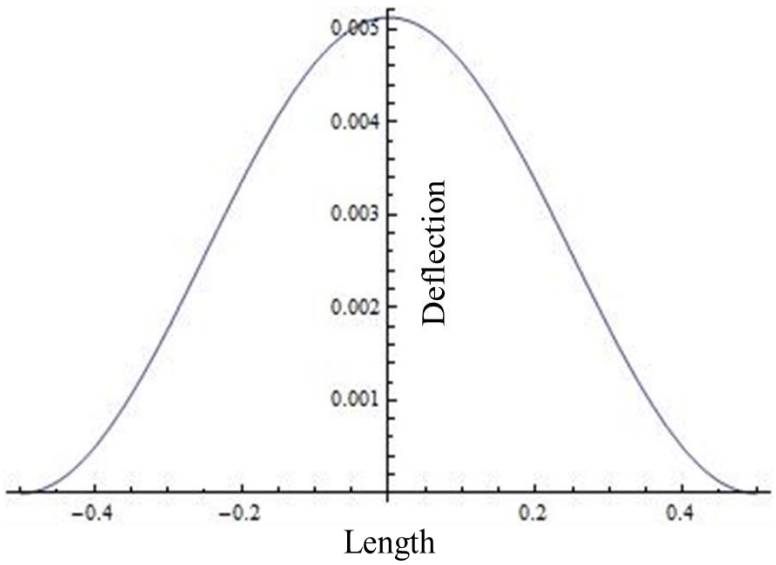

Figure 5.2: Deflection VS length for upper plate (equation 1).

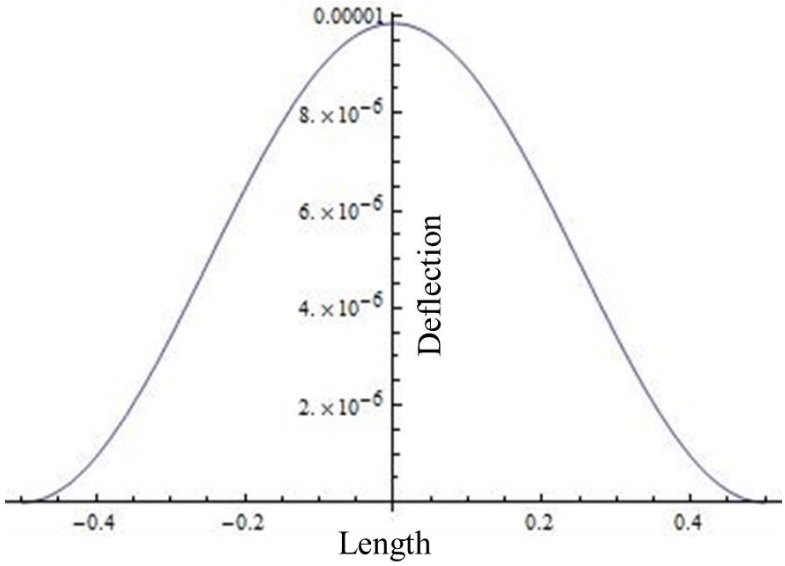

Figure 5.3: Deflection VS length for lower plate (equation 2).

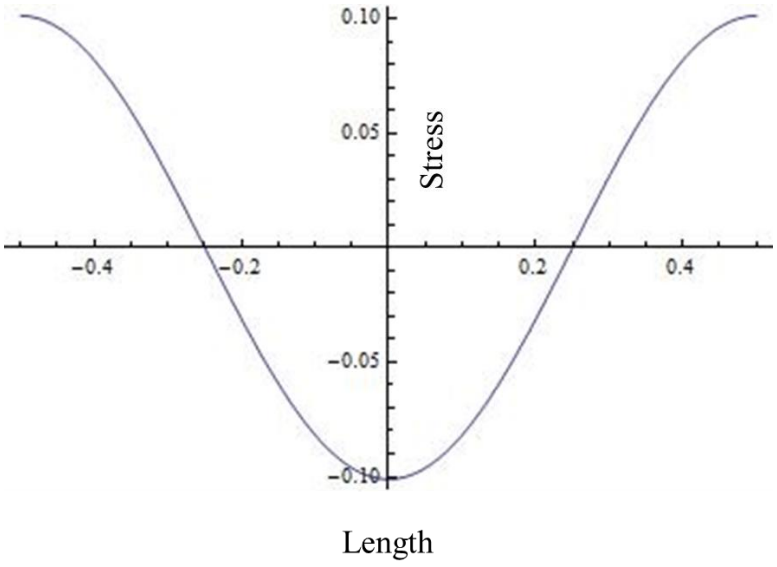

Figure 5.4: Stress VS length for upper plate (equation 9).

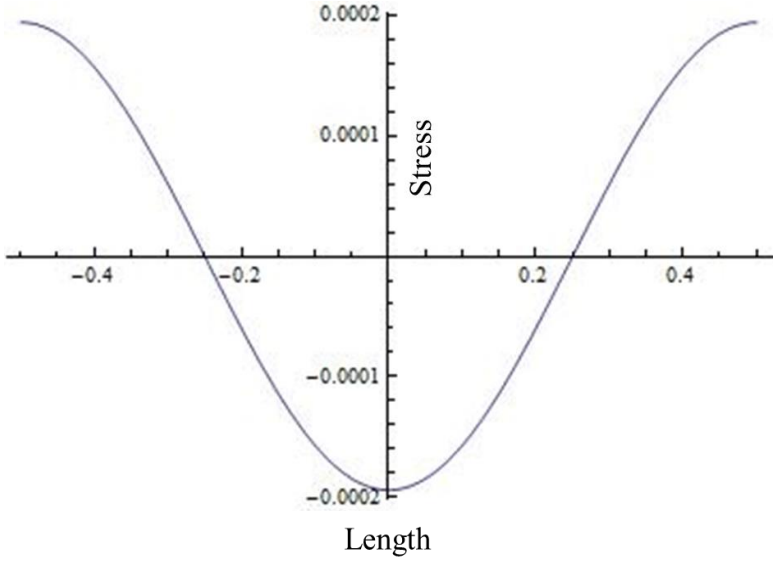

Figure 5.5: Stress VS length for lower plate (equation 10).

Figure 5.6 to 5.10 shows the corresponding figure same as figure 5.1 to 5.5 but in this case one more term on the deflection was added i.e. $W_u = A_1 \left[\text{Cos}\left(\frac{2\pi x}{L}\right) + 1\right] + A_2 \left[\text{Cos}\left(\frac{4\pi x}{L}\right) - 1\right]$ and it is found that by adding more terms on the deflection, the results such as deflection, stress etc. on top and bottom layer.

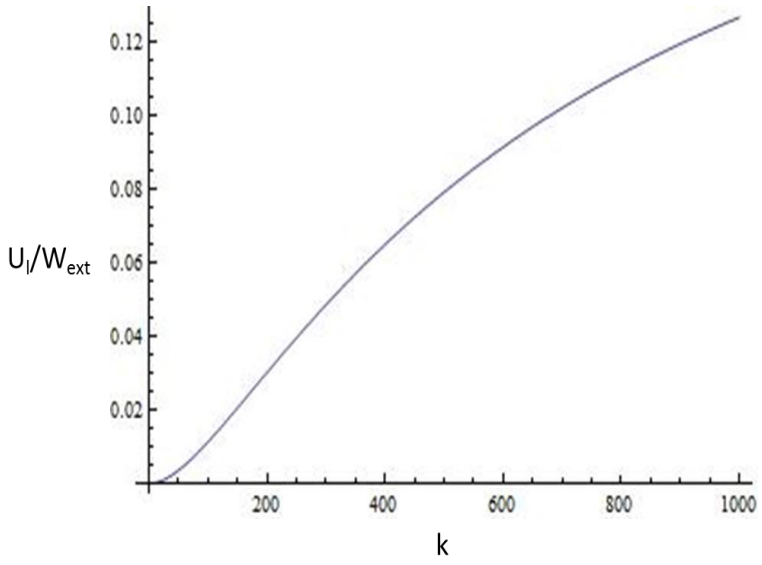

Figure 5.6: Variation of U_l/W_{ext} with respect to k.

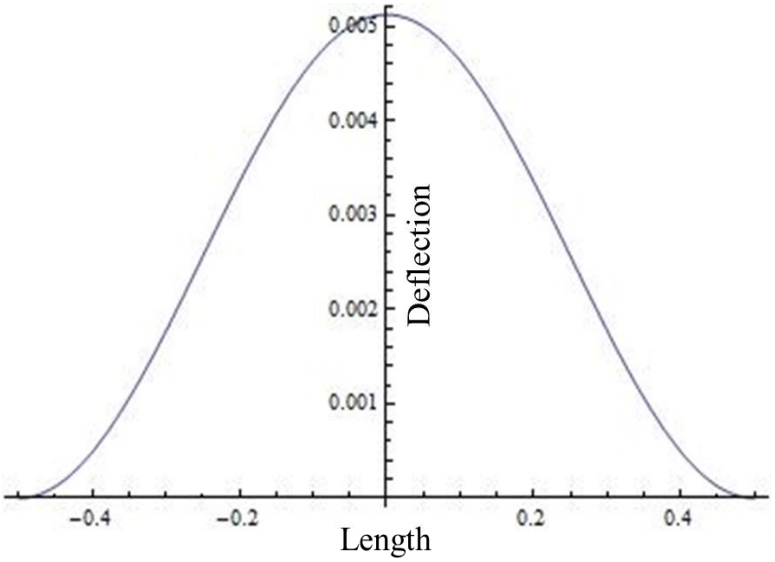

Figure 5.7: Deflection VS length for upper plate.

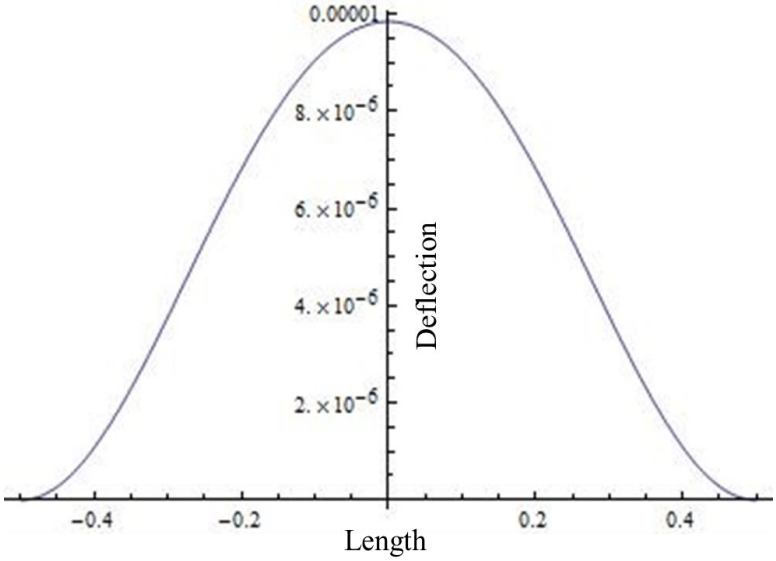

Figure 5.8: Deflection VS length for lower plate.

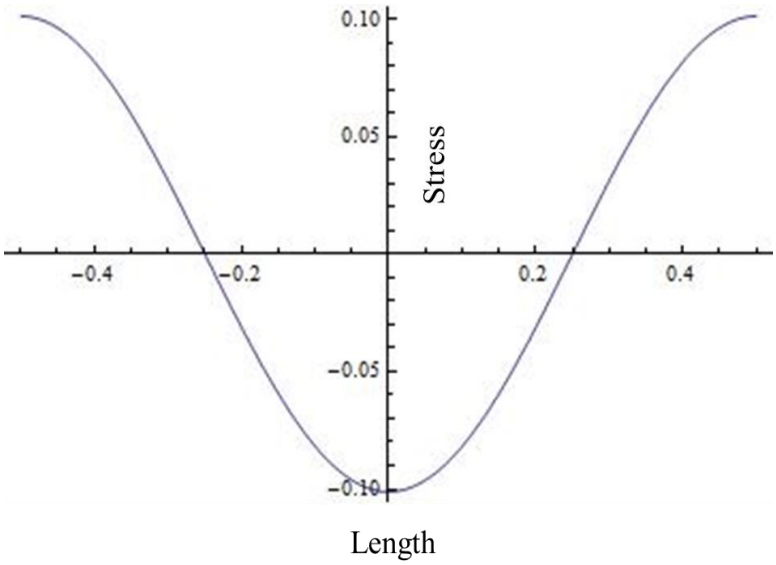

Figure 5.9: Stress VS length for upper plate.

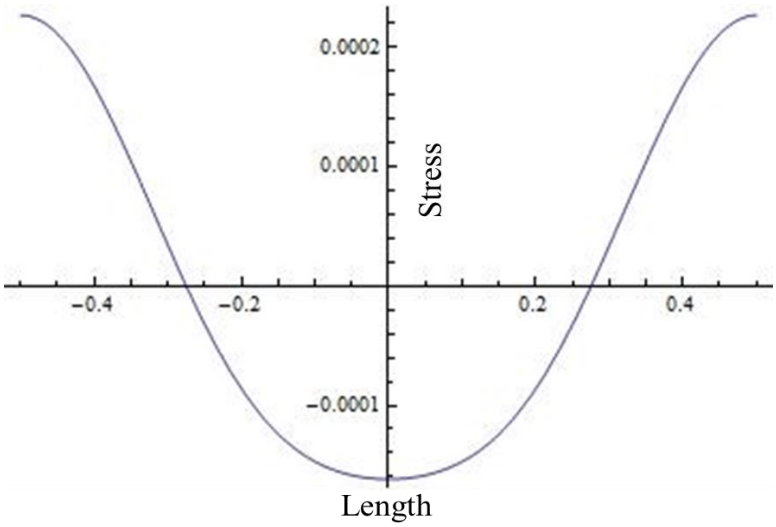

Figure 5.10: Stress VS length for lower plate.

Figure 5.11 shows the variation of $\frac{U_l}{W_{ext}}$ as a function of ratio of EI for the top and bottom layer (E_1I_1/E_2I_2) when EI for the top and bottom layer is different i.e. different material bonded together for different k/E_2I_2. It shows that, for very small value of E_1I_1/E_2I_2, $\frac{U_l}{W_{ext}}$ is very high and it decreases with increase in E_1I_1/E_2I_2. That means when the stiffness (EI) of the top layer is very high compared to the bottom layer then most of the impact energy used to damage the top layer and a very small amount of energy can pass to the bottom layer. Figure 5.12 shows the variation of $\frac{U_l}{W_{ext}}$ as a function of $k/E_2I_2$for bi-material at different E_1I_1/E_2I_2. It shows that when for very large value of k/E_2I_2, the value $\frac{U_l}{W_{ext}}$ is almost constant, i.e. the layered specimen act like as a single specimen.

Illustration 5.2 shows the different dimensions. If we consider the material of the top beam is PMMA and the bottom beam is PC then,

E_1=3.79×109 N/m^2, E_2=2.38×109 N/m^2, $L_1=L_2$=0.076m, $t_1=t_2$=0.006m, t_{AD}=0.0006m and $b_1=b_2=b_{AD}$=0.076 m.

So, $I_1 = I_2 = \frac{1}{12} b_1 t_1^3 = 1.368 \times 10^{-9} m^4$

And, E_1I_1=5184.72 Nm^2, E_2I_2=3255.84 Nm^2

E_{AD}=4.42×10^6 N/m2,

$k = E_{AD} \frac{b_{AD}}{t_{AD}} = 561.13 \times 10^6 N/m^2$

So, $k/E_2I_2f=172.13\times106$ N/m^4.

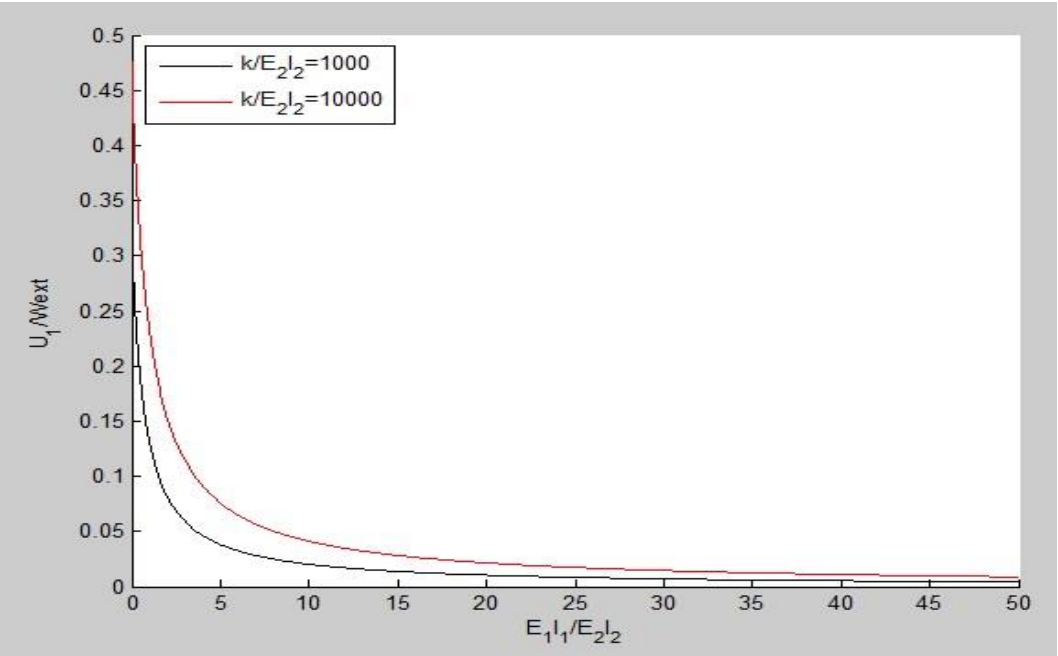

Figure 5.11: U_l/W_{ext} VS $E_1I_1/E_2I_2$for bi-material.

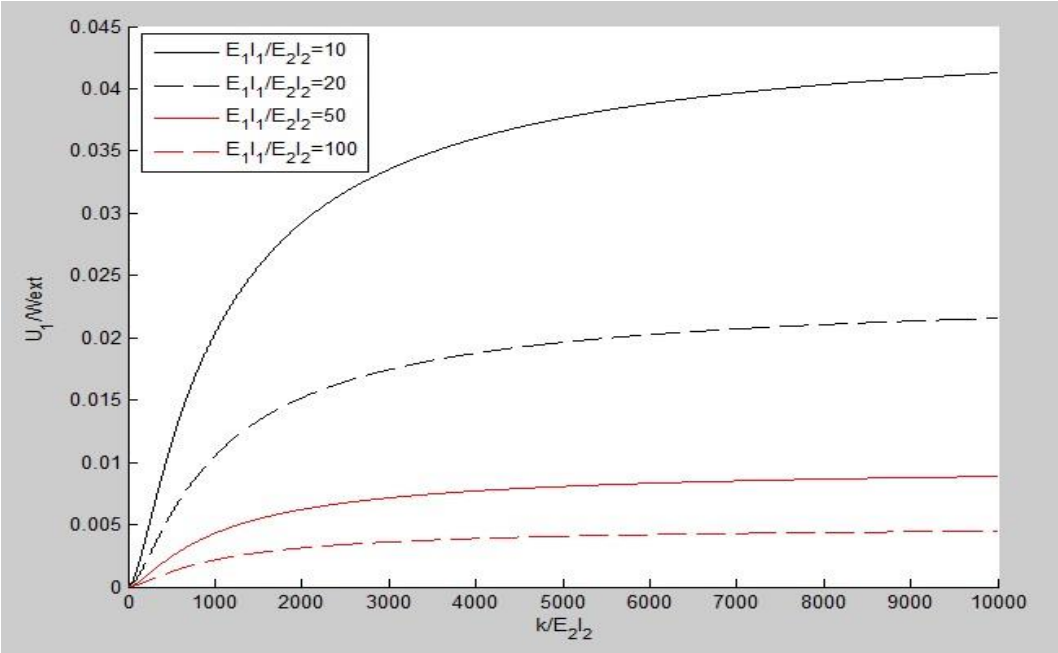

Figure 5.12: U_l/W_{ext} VS $k/E_2I_2$for bi-material.

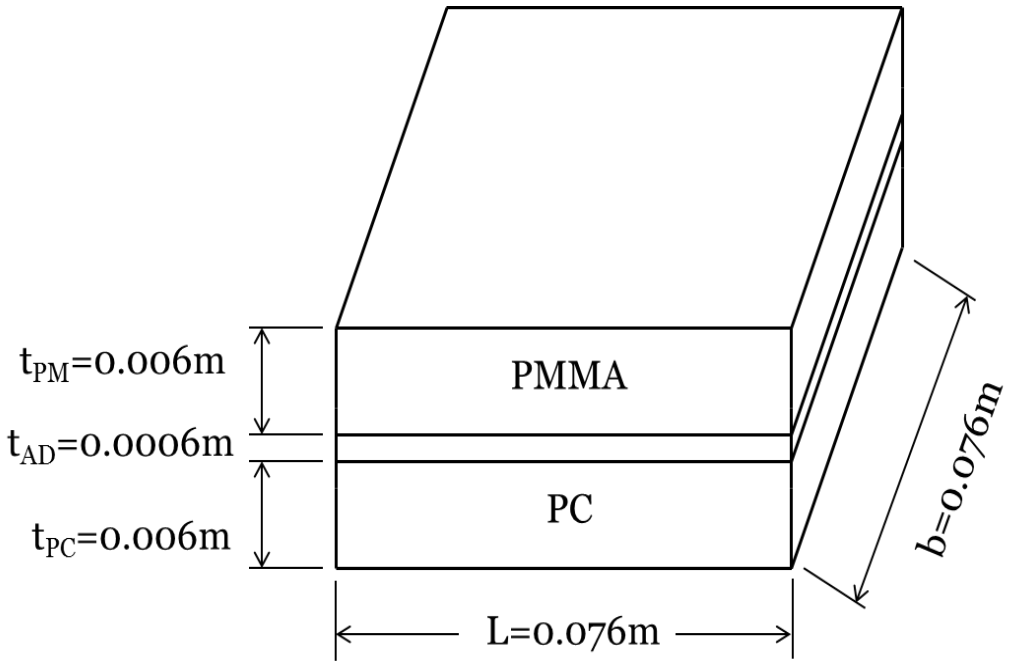

Illustration 5.2: Dimensions of the beam in the analysis.

Chapter 6: Conclusion

Various impact experiments were done on single PC and PMMA specimen at different energy levels. Theoretical and Numerical analysis were also done to predict the impact force and contact duration for a single plate. It is found that a single 11.5 mm thick PMMA plates breaks at 11J impact energy and the crack initiates from the bottom face of the plate i.e. the failure dominated by flexural wave due to low velocity and comparatively large mass of the projectile. The impact resistance of PC is greater than PMMA. Impact was done on single PC plate of thickness 11.5 mm at different energy to find the critical energy at which it fails but it didn't break. Impact experiments were carried out up to 120J impact energy and found that plastic deformation on the impact site but no cracks as seen on the PMMA specimens. From this one can get an idea how tough a PC can be under impact loading because a PMMA specimen of same thickness can break only at 11J impact energy but even 120J impact energy couldn't break PC.

It was found from the experiments that, at low impact energy the single PMMA has greater impact resistance than layered PMMA but at high impact energy, the layered PMMA has greater impact resistance than single PMMA of equal thickness.

Impact on various layered specimens was also done to check the impact resistance of it and it was found that layered material has less impact resistance than the single material of same thickness at low impact energy. But at higher impact energy the layered specimen has greater impact resistance than that of single PMMA specimen of equal thickness.

In case of PC, the impact resistance of layered specimen is greater than the single specimen of same thickness. The maximum impact force is much lower in layered specimen than single specimen. For different material bonded together (PC and PMMA), it was found that PMMA layer always fail irrespective on which layer impact was done.

Analytical solution (chapter 5) shows that in case of layered specimen, the adhesive layer is able to absorb some of the impact energy so the deflection on the top and bottom layer is different.

References

1. Bless, S., T. Chen, and R. Russell. Impact on glass laminates. in 23rd international symposium on ballistics, Tarragona, April. 2007.
2. Bless, S. and T. Chen, Impact damage in layered glass. International Journal of Fracture, 2010. 162(1): p. 151-158.
3. Chen, W.W., Effects of Surface Treatment and Interfacial Strength on the Damage Propagation in Layered Transparent Armor under Impact, 2011, DTIC Document.
4. Grujicic, M., et al., An improved mechanical material model for ballistic soda-lime glass. Journal of materials engineering and performance, 2009. 18(8): p. 1012-1028.
5. Sun, X., et al., Modeling Transparent Armor Behaviors Subject to Projectile Impact, 2008, DTIC Document.
6. Sun, X., et al., Modeling and characterization of dynamic failure of borosilicate glass under compression/shear loading. International Journal of Impact Engineering, 2009. 36(2): p. 226-234.
7. Richardson, M. and M. Wisheart, Review of low-velocity impact properties of composite materials. Composites Part A: Applied Science and Manufacturing, 1996. 27(12): p. 1123-1131.
8. Sjoblom, P.O., J.T. Hartness, and T.M. Cordell, On low-velocity impact testing of composite materials. Journal of Composite Materials, 1988. 22(1): p. 30-52.
9. Shivakumar, K., W. Elber, and W. Illg, Prediction of low-velocity impact damage in thin circular laminates. AIAA journal, 1985. 23(3): p. 442-449.
10. Cantwell, W. and J. Morton, The impact resistance of composite materials—a review. composites, 1991. 22(5): p. 347-362.
11. Abrate, S., Impact on laminated composite materials. Applied mechanics reviews, 1991. 44(4): p. 155-190.
12. Olsson, R., Analytical prediction of large mass impact damage in composite laminates. Composites Part A: Applied Science and Manufacturing, 2001. 32(9): p. 1207-1215.
13. Xu, L.R. and A.J. Rosakis, An experimental study of impact-induced failure events in homogeneous layered materials using dynamic photoelasticity and high-speed photography. Optics and Lasers in Engineering, 2003. 40(4): p. 263-288.
14. Quarterly, A., Army Materials Research: Transforming Land Combat Through New Technologies. AMPTIAC Quart, 2004. 8(4): p. 2-5.

15. Gunnarsson, C.A., T. Weerasooriya, and P. Moy. Measurement of Transient Full-Field, Out-of-Plane Back Surface Displacements of Polycarbonate during Impact. in Proceedings of the 2008 International Congress and Exposition on Experimental Mechanics and Applied Mechanics. 2008.
16. Krishnan, A. and L. Roy Xu, Experimental studies on the interaction among cracks, notches and interfaces of bonded polymers. International Journal of Solids and Structures, 2013.
17. Fischer-Cripps, A.C., Nanoindentation. Vol. 1. 2011: Springer.
18. Abrate, S., Impact on composite structures2005: Cambridge university press.
19. Walley, S., et al., The effect of temperature on the impact behaviour of glass/polycarbonate laminates. International journal of impact engineering, 2004. 30(1): p. 31-53.
20. Golden, J., B. Hammant, and E. Hazell, Effects of molecular weight and strain rate on the flexural properties of polycarbonate. Journal of Applied Polymer Science, 1968. 12(3): p. 557-569.
21. Bauwens, J., Relation between the compression yield stress and the mechanical loss peak of bisphenol-A-polycarbonate in the β transition range. Journal of Materials Science, 1972. 7(5): p. 577-584.
22. Allen, G., D. Morley, and T. Williams, The impact strength of polycarbonate. Journal of Materials Science, 1973. 8(10): p. 1449-1452.
23. Bauwens-Crowet, C., J.-M. Ots, and J.-C. Bauwens, The strain-rate and temperature dependence of yield of polycarbonate in tension, tensile creep and impact tests. Journal of Materials Science, 1974. 9(7): p. 1197-1201.
24. Sacher, E., The impact strength of polycarbonate. Journal of Macromolecular Science, Part B: Physics, 1974. 9(1): p. 163-167.
25. Vincent, P., Impact strength and mechanical losses in thermoplastics. Polymer, 1974. 15(2): p. 111-116.
26. Parvin, M. and J. Williams, Ductile-brittle fracture transitions in polycarbonate. International Journal of Fracture, 1975. 11(6): p. 963-972.
27. Ravetti, R., W. Gerberich, and T. Hutchinson, Toughness, fracture markings, and losses in bisphenol-A polycarbonate at high strainrate. Journal of Materials Science, 1975. 10(8): p. 1441-1448.
28. Goldsmith, W. and F. Katsamanis, Crack propagation in plastics due to impact, in High Velocity Deformation of Solids1978, Springer. p. 195-207.

29. Hillig, W.B., Response of polycarbonate, poly (methylmethacrylate), and epoxy resins to dynamic contact loading I. Experimental results. Polymer Engineering & Science, 1985. 25(6): p. 339-347.
30. Fleck, N., W. Stronge, and J. Liu, High strain-rate shear response of polycarbonate and polymethyl methacrylate. Proceedings of the Royal Society of London. A. Mathematical and Physical Sciences, 1990. 429(1877): p. 459-479.
31. Rietsch, F. and B. Bouette, The compression yield behaviour of polycarbonate over a wide range of strain rates and temperatures. European Polymer Journal, 1990. 26(10): p. 1071-1075.
32. Walley, S., D. Xing, and J. Field, Mechanical properties of three transparent polymers in compression at a very high rate of strain. Impact and Dynamic Fracture of Polymers and Composites", ed. JG Williams and A. Pavan, 1995: p. 289-303.
33. Chiou, K.-C., H.-C. Hsu, and F.-C. Chang, Precrack hysteresis energy in determining polycarbonate ductile-brittle transition. IV. Effect of strain rate. Journal of Applied Polymer Science, 1997. 65(4): p. 655-665.

Glossary

Nomenclature

P	Indentation load
C	Contact Stiffness
h	Indentation depth
n	Fitting parameter
S	Slope of the unloading curve
a	Contact radius
R	Indenter radius
E_r	Reduced modulus
ν, ν_i	Poisson's ratio of target material and indenter
E, E_i	Elastic modulus of target material and indenter
P_{max}	Maximum contact force
C_{IP}, C_{ID}	Contact stiffness during impact and indentation
E	Impact energy
R_{IP}, R_{ID}	Radius of projectile and indenter
E_r^{IP}, E_r^{ID}	Reduced modulus during impact and indentation
M	Mass of projectile
E_b	Energy used in bending
E_s	Energy used in shear
E_m	Energy used in membrane effect
E_c	Energy used in contact
T_c	Contact duration

Vita

Md Shariful Islam, only son of Md Sirajul Islam and Mst. Sufia Khatun, was born on October 18, 1985 in Meherpur, Bangladesh. He completed his secondary school certificate from Dariapur High School and his higher secondary school certificate from Mujibnagar Degree College, Bangladesh and then joined Khulna University of Engineering & Technology (KUET) in 2004 to pursue his Bachelor of Science in Mechanical Engineering. After graduating from KUET he joined at the Department of Mechanical Engineering of the same university on 12th October 2008, and later on 1st January 2012 he promoted to Assistant Professor. There he was responsible for taking undergraduate class, he was also involved himself in the departmental Consultancy, Research and Testing Services (CRTS). He took admission in the University of Texas at El Paso (UTEP) in January 2012 to pursue his Master of Science degree in mechanical Engineering. He was working as a Graduate Teaching Assistant for the department. He also worked as a Research Assistant. His research was focused on a damage-trap interfacial design to improve impact resistance of polymers.

Permanent address: Village: Purondorpur, P.O. Dariapur
P.S. Mujibnagar, Dist. Meherpur, Bangladesh

This thesis/dissertation was typed by Md Shariful Islam.